Synapses in oligodendrocyte precursor cells are dynamic and contribute to Ca^{2+} activity

Jiaxing Li[1, *], Tania Miramontes[1], Tim Czopka[2], Kelly Monk[1, *]

1 Vollum Institute, Oregon Health & Science University, Portland, OR, USA

2 Centre for Clinical Brain Sciences, University of Edinburgh, Edinburgh, UK

* Corresponding authors

Cell-cell interactions are critical to central nervous system (CNS) structure and function. Direct neuron-neuron interactions occur via synapses, but only one type of neuron-glia synapse is known to exist: those formed between neurons (pre-) and oligodendrocyte precursor cells (OPCs) (post-)[1,2]. These synapses are thought to bridge neuronal activity to OPCs, which are critical for developmental myelination and adult motor learning[3]. However, the composition and assembly of neuron-OPC synapses and their *in vivo* functions remain largely unclear. Here, using zebrafish to label postsynaptic organizers PSD-95 and Gephyrin in OPCs, we found that synapses in OPCs possess dynamic assembly properties and are developmentally regulated. We also found that synapses and voltage-gated Ca^{2+} channels (VGCCs) play important roles in driving intrinsic OPC Ca^{2+} activity that occurs mainly in microdomains, while evoked synaptic release has a limited role that diminishes through development. Finally, disrupting a key synaptic gene, *neuroligin3b,* specifically in OPCs impairs OPC differentiation and subsequent myelination. Our results establish an *in vivo* model of dynamic neuron-OPC synapses mediating intrinsic OPC Ca^{2+} activity and impacting OPC differentiation, pointing to plastic neuron-OPC interactions and synapse-dependent and -independent Ca^{2+} pathways in OPCs.

45 Neuron-OPC synapse assembly and disassembly is mysterious. This is largely due to lack of
46 labeling methods, especially *in vivo*. The composition of these synapses is also largely unknown,
47 with the exception of some neurotransmitter and synaptic receptors (*e.g.*, glutamatergic and
48 GABAergic) that have been revealed by pharmacology and electrophysiology[3]. OPCs exhibit
49 heterogeneity[4,5], raising the question of whether synapse assembly differs among OPCs. Unlike
50 canonical postsynaptic cells (*e.g.*, neurons and muscle cells), OPCs migrate and constantly
51 remodel their processes, and many OPCs differentiate and transform these processes into
52 myelin sheaths[3]. Therefore, OPCs may employ special mechanisms of synapse assembly to
53 accommodate their unique biology, a notion further supported by transcriptomic studies
54 suggesting different synaptic gene expression in OPCs from neurons[6,7]. These transcriptomic
55 studies, however, do indicate the presence of PSD-95 (a major MAGUK family member) and
56 Gephyrin in OPCs (Extended Data Fig. 1)[6], which are abundant postsynaptic scaffold proteins at
57 excitatory and inhibitory neuron-neuron synapses, respectively[8], making them promising
58 candidates for neuron-OPC synapse labeling.

59 Previous *ex vivo* rodent studies linked axon stimulation and neuron-OPC synapses to
60 Ca^{2+} rise in oligodendrocyte lineage cell somas and proximal processes[9–11]. While these studies
61 demonstrate the capacity of neuron-OPC synapses to induce OPC Ca^{2+} activity, it remains
62 unknown if these synapses contribute to generating intrinsic OPC Ca^{2+} activity *in vivo*.
63 Furthermore, recent *in vivo* zebrafish studies revealed intrinsic Ca^{2+} events in microdomains of
64 OPC processes[4,12], but the role of synapses in generating these events is largely unknown. Here
65 we leveraged zebrafish to study synapse assembly mechanisms in OPCs *in vivo* and to address
66 the role of synapses in OPC biology and intrinsic Ca^{2+} activity.

67 ***Postsynaptic structures (PSSs) in OPCs are dynamic, assemble at preferential locations, and***
68 ***many lack presynaptic structure alignment.***

69 We generated PSD-95-GFP and GFP-Gephyrin constructs and drove their expression
70 with a pan-oligodendrocyte lineage promoter (*sox10*, see Methods). At 3 days post fertilization
71 (dpf) in the spinal cord, we found both markers present in punctate and cytosolic forms in OPCs
72 (Fig. 1a, see methods for OPC identification), consistent with patterns observed in neurons[13,14],
73 with OPC puncta size resembling that of neurons (Fig. 1a-b and Extended Data Fig. 2a). We
74 detected 29 ± 4.4 (N=18) PSD-95-GFP and 27 ± 3.5 (N=14) GFP-Gephyrin puncta per OPC.
75 Through immunohistochemistry (IHC), we verified the presence of MAGUK (and PSD-95) and
76 Gephyrin puncta in spinal cord OPCs (Extended Data Fig. 3). We found similar Gephyrin puncta
77 number between *in vivo* imaging and IHC, and higher PSD-95 puncta number by *in vivo* imaging
78 than by IHC (Extended Data Fig. 3h), possibly due to increased synaptogenesis with PSD-95
79 overexpression[15]. Despite the overexpression caveat, the IHC results verified our *in vivo*
80 methods for labeling PSS puncta in OPCs. Through time-lapse imaging, we found that the
81 number of PSS puncta per cell remains stable in a neuron, but fluctuates in an OPC over 30
82 minutes of observation (Fig. 1c and Supplementary Videos 1-4). The puncta of PSD-95-GFP and
83 GFP-Gephyrin in OPCs are considerably shorter-lived than in neurons (Fig. 1d). Many puncta in
84 neurons last more than 10,000 seconds; conversely, we found no such stable puncta in OPCs
85 (Fig. 1e). While some PSS puncta in OPCs appear or disappear as processes remodel (Extended
86 Data Fig. 2b and Supplemental Video 3), others do when processes are relatively stable
87 (Extended Data Fig. 2c-d and Supplemental Video 1). Some PSS puncta in OPCs appear
88 preferentially at certain locations, verified by frequency maps (Fig. 1f-g). Further analysis

89 revealed that PSS puncta in these “hotspots” repeatedly assemble and disassemble (10-12
90 “hotspots” per cell, Fig. 1h and Extended Data Fig. 2c-d). Notably, we observed this
91 phenomenon in not only dynamic processes but also stable processes (Extended Data Fig. 2c-d),
92 suggesting that the repeatedly assembled and disassembled “hotspots” are not simply caused
93 by process instability.

94 Next, we tested whether these dynamic PSS puncta form complete synapses by
95 examining their alignment with presynaptic structures (pan-presynaptic marker Synapsin 1/2[16]).
96 We found nearly a 50% alignment rate for MAGUK and Gephyrin in OPCs and a reduced
97 colocalization ratio between pre- and post-synaptic staining compared to neurons (Extended
98 Data Fig. 4). This suggests that nearly 50% of PSSs found in OPCs are part of a functional
99 synapse unit while the rest lack synaptic partners. Similar non-aligned PSSs have been reported
100 in developing neurons and are considered to be immature[17,18]. From these data, we conclude
101 that PSSs in OPCs are more dynamic than neurons, assemble and disassemble frequently, and
102 that many are likely immature.

103

104 ***PSSs number in OPCs are developmentally regulated, with few regional and subgroup***
105 ***differences.***

106 Given previously reported OPC heterogeneity[4,5], we wondered if PSSs in OPCs are
107 regulated spatially, temporally, and/or between subgroups. Using IHC, we found that MAGUK
108 puncta numbers are similar across CNS regions, while Gephyrin puncta number is significantly
109 higher in the forebrain and midbrain compared to the spinal cord (Extended Data Fig. 5a),
110 suggesting a preference of OPCs to form synapses with inhibitory neurons in the brain. Two

111 subgroups of OPCs have been reported in zebrafish spinal cord that exhibit distinct
112 transcriptional profiles and myelination potential[4]. Despite these differences, both subgroups
113 possess similar PSS numbers (Extended Data Fig. 5b-c).
114 We found that both MAGUK (and PSD-95) and Gephyrin puncta numbers in OPCs
115 increase as animals develop using *in vivo* imaging and IHC (Fig. 2a-b). Time-lapse imaging of
116 OPCs revealed that coincident with differentiation, PSS number is reduced (Fig. 2c-d), which
117 could account for reduced synaptic inputs previously reported at this stage[19,20]. In cases where
118 we observed differentiating oligodendrocytes that possess both processes and myelin sheaths,
119 puncta were almost exclusively in processes (Fig. 2e), suggesting preferential localization of
120 PSSs to processes rather than nascent myelin sheaths. These results show that PSS number in
121 OPCs increases as animals develop and decreases upon OPC differentiation.
122
123 ***Synapses and VGCCs contribute to generating intrinsic OPC Ca^{2+} activity in vivo.***
124 To investigate the role of synapses in intrinsic OPC Ca^{2+} activity *in vivo*, we employed a plasma-
125 membrane-targeting GCaMP6s (See Methods). At single cell resolution, we found that the
126 majority (99%) of Ca^{2+} events in OPCs occur in microdomains on processes (Fig. 3a): we
127 recorded 624 local events (Supplementary Video 5) and 6 somal events (Supplementary Video 6)
128 from 180 cells, 107 fish, 30 hours imaging period. To test if intrinsic OPC Ca^{2+} activity is
129 mediated by synapses, we first examined the proximity between Ca^{2+} events and synapses,
130 visualized by a presynaptic marker, synaptophysin-TagRFP[4]. Through 3D analysis, we found that
131 34 ± 9% of Ca^{2+} microdomains are in close proximity (<0.1 µm) to synaptophysin-TagRFP puncta
132 at 5 dpf (Fig. 3b-e). In some cases, we observed Ca^{2+} events initiate from a "puncta"-like region

133 in close proximity to synapses (Extended Data Fig. 6a-c). Next, we blocked synaptic release by
134 expressing tetanus toxin light chain (TeTxLc)-tdtomato[21] in axons (Fig. 3f). Compared to OPCs
135 neighboring few TeTxLc-expressing axons (< 4), OPCs neighboring many TeTxLc-expressing
136 axons (> 4) showed significantly reduced frequency of Ca^{2+} activity, peak amplitude, basal signal
137 intensity, and microdomain length (Fig. 3g and Extended Data Fig. 6d). Together, these results
138 establish an *in vivo* role for synapses in generating intrinsic OPC Ca^{2+} activity that mainly occurs
139 in microdomains.

140 We next asked what receptors or channels at synapses mediate intrinsic OPC Ca^{2+}
141 activity. We tested NMDA receptors, CP-AMPA receptors, and VGCCs, as suggested by previous
142 *ex vivo* studies[9–11], by administering their antagonists (AP5, IEM-1460, and cadmium,
143 respectively) via ventricle injection as described previously[12] (Fig. 3h). We confirmed successful
144 drug delivery: injections induced paralysis by 3 minutes post-injection (AP5, 15/19; IEM-1460,
145 14/14; cadmium, 9/10), and dextran co-injected with antagonist (dextran MW3000, larger than
146 the antagonists) diffused and encompassed OPCs prior to imaging in all cases (45/45) (Extended
147 Data Fig. 6e). We found that AP5 and IEM-1460 did not inhibit the overall Ca^{2+} activity (Fig. 3i
148 and Extended Data Fig. 6f). In contrast, cadmium administration significantly reduced
149 microdomain number per OPC (4.4 ± 1.0 to 2.0 ± 0.5) as well as the frequency of Ca^{2+} activity
150 per microdomain (1.8 ± 0.2 to 0.9 ± 0.2 x 10^{-3} Hz) (Fig. 3i, Extended Data Fig. 6f, Supplementary
151 Video 7-8). The overall 50-55% reduction in both analyses suggests that VGCCs, but not NMDA
152 or CP-AMPA receptors, play a critical role in generating intrinsic OPC Ca^{2+} activity *in vivo*.
153

154 ***Neuronal activity and evoked synaptic release play a limited role in intrinsic OPC Ca^{2+} activity***

155 ***during early development.***

156 Expanding from a previous study[12], we examined the role of neuronal activity and evoked

157 synaptic release in driving intrinsic OPC Ca^{2+} activity at two developmental stages (3 dpf, when

158 OPCs initiate differentiation and 5 dpf, when many OPCs complete differentiation[22]). Similar to

159 previous results with 3 dpf larvae[12], upon ventricle injection (Fig. 3h) of tetrodotoxin (TTX,

160 sodium channel blocker), OPCs exhibited reductions in the frequency of Ca^{2+} activity (Extended

161 Data Fig. 7a and Supplementary Video 9). In addition, we observed reduced microdomain

162 number per OPC (3.0 ± 0.4 *vs.* 2.2 ± 0.3) and peak amplitude (2.1 ± 0.2 *vs.* 1.6 ± 0.1 fold)

163 (Extended Data Fig. 7a). The overall 25-33% reduction in these analyses suggests a partial

164 requirement of neuronal activity and evoked synaptic release for intrinsic OPC Ca^{2+} activity.

165 However, we found no such requirement at 5 dpf (Extended Data Fig. 7a). We excluded the

166 possibility of ineffective TTX delivery in three ways. We observed larval paralysis within 3

167 minutes post-injection (30/30), a complete block of motor neuron Ca^{2+} activity (Extended Data

168 Fig. 7b-c), and dextran co-injected with TTX (dextran MW3000, larger than TTX) surrounded the

169 imaged OPCs (120/120) (Extended Data Fig. 7d). Therefore, our results point to a limited role of

170 neuronal activity and evoked synaptic release in driving intrinsic OPC Ca^{2+} activity, which

171 diminishes over development. These results also suggest that the role of synapses we observed

172 (Fig. 3) were likely mediated by spontaneous synaptic release.

173

174 ***Synaptic component nlgn3b is important for oligodendrocyte differentiation and myelination.***

175 The role of neuron-OPC synapses in development is unclear due to diverse and
176 sometimes conflicting results of individual receptor disruption[23–26]. To overcome this, we
177 targeted *neuroligin3* (*nlgn3*), which localizes to both excitatory and inhibitory synapses,
178 regulates neuronal synapse structure and function[27], and is enriched in OPCs (Extended Data Fig.
179 1)[6]. We developed and verified a cell-specific CRISPR/Cas9-mediated gene disruption system
180 (Extended Data Fig. 8) and targeted the duplicated *nlgn3* genes (*nlgn3a* and *nlgn3b*) in zebrafish.
181 We observed an increased OPC to myelinating oligodendrocyte ratio in *nlgn3b*-targeted cells at
182 3 dpf (ctrl 3:61, *nlgn3a* 0:19, *nlgn3b* 9:25) and at 5 dpf (ctrl 1:66, *nlgn3a* 2:56, *nlgn3b* 18:47,
183 Extended Data Fig. 8e), suggesting that loss of *nlgn3* disrupts proper OPC differentiation. At 5
184 dpf, almost all myelinating oligodendrocytes in control animals possess only myelin sheaths. In
185 contrast, several *nlgn3b*-disrupted oligodendrocytes possess both myelin sheaths and
186 cytoplasmic processes with abnormal trapezoidal structures (ctrl: 0 out of 67, *nlgn3a*: 0 out of
187 58, *nlgn3b*: 3 out of 65, Fig. 4a and extended Data Fig. 8f), indicating developmental defects
188 when Neuroligin3b is lost. Additionally, disruption of *nlgn3b* leads to reduced total length of
189 myelin sheaths per oligodendrocyte at 3 dpf (Fig. 4b), which was largely resolved by 5 dpf (Fig.
190 4c), suggesting a temporary delay in myelin sheath formation. Together, these results suggest a
191 role for Neuroligin3 specifically and neuron-OPC synapses more broadly in oligodendrocyte
192 differentiation and myelination.
193

194 **Discussion**

195 The landmark discovery of neuron-OPC synapses has inspired several studies to examine
196 their properties with electrophysiology and EM[3], yet we still lack basic understanding of their

197 assembly and function. Here, we identified PSSs composed of MAGUK (PSD-95) and Gephyrin in
198 zebrafish OPCs and revealed unique synapse features: dynamic assembly, lack of consistent
199 synaptic partners, and frequent assembly at specific locations. Interestingly, these features
200 have also been reported in some neurons, although to a lesser extent[17,18,28,29]. These synapse
201 features may enable flexible neuron-OPC synapse formation in tune with neuronal inputs.
202 Development influences synapse formation in OPCs: PSS number doubles within a few days
203 during animal development and decreases upon OPC differentiation and myelin sheath
204 formation. Meanwhile, OPC development seems to require proper synapse formation, revealed
205 by oligodendrocyte-specific disruption of *nlgn3b*. Together, these findings pinpoint a
206 bidirectional and mutually influencing relationship between dynamic synapse assembly and
207 OPC development (Fig. 4d) and a newly discovered developmental role of *nlgn3b*, previously
208 shown to promote glioma growth[30].

209 Several previous studies investigated synaptic mechanisms underlying Ca^{2+} elevation in
210 OPCs[9–11], yet the role of synapses in driving intrinsic OPC Ca^{2+} activity *in vivo* and in
211 microdomains was never explored. Our work suggests the requirement of synapses in
212 generating intrinsic OPC Ca^{2+} activity that mainly occur in microdomains. We further showed
213 that Ca^{2+} influx is likely mediated by VGCCs, but not CP-AMPA or NMDA receptors. This is in
214 contrast with a previous *ex vivo* study[9] and could be explained by the different mechanisms
215 underlying somal *vs.* microdomain Ca^{2+} events. To our surprise, neuronal activity and evoked
216 synaptic release contribute moderately to intrinsic OPC Ca^{2+} activity at 3 dpf but not 5 dpf.
217 Considering that OPC differentiation initiates at 3 dpf, it suggests an OPC sensitivity to neuronal
218 activity through Ca^{2+} signaling at this critical developmental stage. Overall, our results establish

219 an *in vivo* model of intrinsic OPC Ca^{2+} activity: synapses, likely through spontaneous release,
220 play an important role with evoked release and neuronal activity contributing during early
221 development.
222
223 **References**

224 1. Bergles, D. E., Roberts, J. D. B., Somogyl, P. & Jahr, C. E. Glutamatergic synapses on
225 oligodendrocyte precursor cells in the hippocampus. *Nature* **405**, 187–191 (2000).
226 2. Lin, S. C. & Bergles, D. E. Synaptic signaling between GABAergic interneurons and
227 oligodendrocyte precursor cells in the hippocampus. *Nat. Neurosci.* **7**, 24–32 (2004).
228 3. Bergles, D. E. & Richardson, W. D. Oligodendrocyte development and plasticity. *Cold*
229 *Spring Harb. Perspect. Biol.* **8**, a020453 (2016).
230 4. Marisca, R. *et al.* Functionally distinct subgroups of oligodendrocyte precursor cells
231 integrate neural activity and execute myelin formation. *Nat. Neurosci.* **23**, 363–374
232 (2020).
233 5. Spitzer, S. O. *et al.* Oligodendrocyte Progenitor Cells Become Regionally Diverse and
234 Heterogeneous with Age. *Neuron* **101**, 459-471.e5 (2019).
235 6. Zhang, Y. *et al.* An RNA-sequencing transcriptome and splicing database of glia, neurons,
236 and vascular cells of the cerebral cortex. *J. Neurosci.* **34**, 11929–11947 (2014).
237 7. Marques, S. *et al.* Oligodendrocyte heterogeneity in the mouse juvenile and adult central
238 nervous system. *Science (80-.).* **352**, 1326–1329 (2016).
239 8. Sheng, M. & Kim, E. The postsynaptic organization of synapses. *Cold Spring Harb.*
240 *Perspect. Biol.* **3**, a005678–a005678 (2011).

241 9. Barron, T. & Kim, J. H. Neuronal input triggers Ca2+ influx through AMPA receptors and
242 voltage-gated Ca2+ channels in oligodendrocytes. *Glia* **67**, 1922–1932 (2019).
243 10. Sun, W., Matthews, E. A., Nicolas, V., Schoch, S. & Dietrich, D. NG2 glial cells integrate
244 synaptic input in global and dendritic calcium signals. *Elife* **5**, (2016).
245 11. Hamilton, N., Vayro, S., Wigley, R. & Butt, A. M. Axons and astrocytes release ATP and
246 glutamate to evoke calcium signals in NG2-glia. *Glia* **58**, 66–79 (2010).
247 12. Krasnow, A. M., Ford, M. C., Valdivia, L. E., Wilson, S. W. & Attwell, D. Regulation of
248 developing myelin sheath elongation by oligodendrocyte calcium transients in vivo. *Nat.*
249 *Neurosci.* **21**, 24–30 (2018).
250 13. Yoshii, A. & Constantine-Paton, M. BDNF induces transport of PSD-95 to dendrites
251 through PI3K-AKT signaling after NMDA receptor activation. *Nat. Neurosci.* **10**, 702–711
252 (2007).
253 14. Meier, J. & Grantyn, R. A Gephyrin-Related Mechanism Restraining Glycine Receptor
254 Anchoring at GABAergic Synapses. *J. Neurosci.* **24**, 1398–1405 (2004).
255 15. Nikonenko, I. *et al.* PSD-95 promotes synaptogenesis and multiinnervated spine
256 formation through nitric oxide signaling. *J. Cell Biol.* **183**, 1115–1127 (2008).
257 16. Easley-Neal, C., Fierro, J., Buchanan, J. A. & Washbourne, P. Late Recruitment of Synapsin
258 to Nascent Synapses Is Regulated by Cdk5. *Cell Rep.* **3**, 1199–1212 (2013).
259 17. Gerrow, K. *et al.* A preformed complex of postsynaptic proteins is involved in excitatory
260 synapse development. *Neuron* **49**, 547–562 (2006).
261 18. Panzer, J. A. *et al.* Neuromuscular synaptogenesis in wild-type and mutant zebrafish. *Dev.*
262 *Biol.* **285**, 340–357 (2005).

263 19. Kukley, M., Nishiyama, A. & Dietrich, D. The fate of synaptic input to NG2 glial cells:
264 Neurons specifically downregulate transmitter release onto differentiating
265 oligodendroglial cells. *J. Neurosci.* **30**, 8320–8331 (2010).
266 20. De Biase, L. M., Nishiyama, A. & Bergles, D. E. Excitability and synaptic communication
267 within the oligodendrocyte lineage. *J. Neurosci.* **30**, 3600–3611 (2010).
268 21. Koudelka, S. *et al.* Individual Neuronal Subtypes Exhibit Diversity in CNS Myelination
269 Mediated by Synaptic Vesicle Release. *Curr. Biol.* **26**, 1447–1455 (2016).
270 22. Almeida, R. & Lyons, D. Oligodendrocyte development in the absence of their target
271 axons in Vivo. *PLoS One* **11**, (2016).
272 23. Balia, M., Benamer, N. & Angulo, M. C. A specific GABAergic synapse onto
273 oligodendrocyte precursors does not regulate cortical oligodendrogenesis. *Glia* **65**, 1821–
274 1832 (2017).
275 24. de Biase, L. M. *et al.* NMDA receptor signaling in oligodendrocyte progenitors is not
276 required for oligodendrogenesis and myelination. *J. Neurosci.* **31**, 12650–12662 (2011).
277 25. Zonouzi, M. *et al.* GABAergic regulation of cerebellar NG2 cell development is altered in
278 perinatal white matter injury. *Nat. Neurosci.* **18**, 674–682 (2015).
279 26. Lundgaard, I. *et al.* Neuregulin and BDNF Induce a Switch to NMDA Receptor-Dependent
280 Myelination by Oligodendrocytes. *PLoS Biol.* **11**, (2013).
281 27. Krueger-Burg, D., Papadopoulos, T. & Brose, N. Organizers of inhibitory synapses come of
282 age. *Curr. Opin. Neurobiol.* **45**, 66–77 (2017).
283 28. Wierenga, C. J., Becker, N. & Bonhoeffer, T. GABAergic synapses are formed without the
284 involvement of dendritic protrusions. *Nat. Neurosci.* **11**, 1044–1052 (2008).

285 29. Villa, K. L. *et al.* Inhibitory Synapses Are Repeatedly Assembled and Removed at
286 Persistent Sites In Vivo. *Neuron* **89**, 756–769 (2016).
287 30. Venkatesh, H. S. *et al.* Neuronal activity promotes glioma growth through neuroligin-3
288 secretion. *Cell* **161**, 803–816 (2015).
289

290 ## Methods

291 ***Zebrafish lines and husbandry***

292 We used the following existing zebrafish lines and strains: *Tg(sox10:Kalta4)*[31], *Tg(olig1:Kalta4)*[4],
293 *Tg(huc:synaptophysin-tagRFP)*[4], *Tg(olig2:dsRed)*, *Tg(sox10:GFP-caax)*, *nacre*, and AB. The
294 following lines were newly generated for this study: *Tg(10xUAS:myrGCaMP6s)*,
295 *Tg(olig1:myrGCaMP6s), Tg(10xUAS:myrGFP), Tg(10xUAS:myrmScarletI-p2A-Cas9, U6:ctrl-*
296 *sgRNA1;U6:ctrl-sgRNA2), Tg(10xUAS:myrmScarletI-p2A-Cas9, U6:nlgn3a*^{ex1}*-*
297 *sgRNA;U6:nlgn3a*^{ex4}*-sgRNA), Tg(10xUAS:myrmScarletI-p2A-Cas9, U6:nlgn3b*^{ex1}*-*
298 *sgRNA;U6:nlgn3b*^{ex3}*-sgRNA)*. All experimental fish were crossed into the *nacre* background for
299 optimal optics without pigmentation. The Kalta4/UAS system allows sparse labeling and single
300 cell analysis. The genotypes of fish used for each experiment were indicated in figure legends or
301 Supplementary Table 3. All animals were kept at 28° C with a 14 h/10 h light/dark cycle.
302 Larvae and juveniles were nurtured with rotifer suspension and dry food (Gemma 75 and 150,
303 respectively). Adults were fed with a combination of brine shrimp and dry food (Gemma 300).
304 All zebrafish experiments and procedures were performed in compliance with institutional
305 ethical regulations for animal testing and research at Oregon Health and Science University

306 (OHSU). Experiments were approved by the Institutional Animal Care and Use Committee of
307 OHSU. Animal and cell number were indicated in figure legends or Supplementary Table 2.

308 ***Tissue sectioning and immunohistochemistry***

309 To prepare sagittal and transverse sections, zebrafish larvae at indicated stages were first
310 anesthetized with tricaine and then fixed in 4% PFA, 0.1% Triton at 4° C overnight. Heads and
311 tails were removed to enable better penetration of fixative. The fish were then washed in PBS,
312 0.1% Triton for 5 minutes and passed in 10%, 20%, and 30% sucrose in PBS, followed by OCT
313 embedding and cryosectioning of 20-25 µm slices. The sections were brought to room
314 temperature for 45 min and rehydrated in PBS, 0.2% Triton for 1 hour. 3% BSA, 5% NGS, 0.2%
315 Triton in PBS was used as blocking buffer. Primary antibodies: chicken anti-GFP (Invitrogen
316 A10262), 1:1000, mouse anti-Pan-MAGUK (NeuroMab K28/86) 1:500, mouse anti-Gephyrin
317 (Synaptic Systems 147011) 1:1000, rabbit anti-Synapsin 1/2 (Synaptic Systems 106002) 1:1000,
318 mouse anti PSD-95 6G6-1C9 (MAB1596) 1:1000. Secondary antibodies: A488 anti-chicken, A594
319 anti-rabbit, A647 anti-mouse IgGI, A647 anti-mouse (Thermo Fisher). The stained samples were
320 mounted in prolong Glass (Invitrogen P36980) for at least a day before imaging.

321 ***Plasmid construction***

322 In zebrafish, *gephyrin* is duplicated (*gephyrina* and *gephyrinb*), and there are multiple isoforms
323 for both genes. All isoforms are almost identical in protein sequence except for the inclusion or
324 exclusion of C3 and C4 cassettes. We amplified several isoforms from cDNA and decided to
325 follow up *gephyrinb* isoform X6 (XM_021468341) because it encodes a protein that is 96%
326 identical and 98% similar to the rat P1 isoform (NP_074056.2)[32] that has been used to track

327 synapses previously, and, *gephyrina* isoform X11 (XM_017351650.2) because it contains a C3
328 cassette previously reported to be present in glia cells[33].
329 Total RNA was extracted from 3 dpf zebrafish AB larvae (50 fish) using RNAeasy Plus Kit
330 (Qiagen 74134). cDNA was synthesized using SuperScript IV Reverse Transcriptase (Invitrogen).
331 2 sets of primers (Supplementary Table 1) were used to clone the full length *gephyrina* and
332 *gephyrinb* using high fidelity Q5 DNA polymerase, followed by A-addition and TA cloning into
333 pCRII-TOPO backbones. Using Gibson assembly (NEB E5510S), we added EGFP to the 5' end and
334 a linker GGGGSGGGGSGGGGS in between, and integrated it into pCS 2.1 backbones with an
335 AVRII digestion site. The 5' end was chosen based on previous imaging studies[32]. In transient
336 injections, GFP-Gephyrina and GFP-Gephyrinb exhibit similar expression profiles; therefore, we
337 used GFP-Gephyrinb for our studies and refer to the GFP-3xGGGGS-Gephyrinb as GFP-
338 Gephyrinb throughout. Using Gateway BP reaction (Invitrogen 11786100), we generated
339 pME_ATG-GFP-Gephyrinb-TAA. Using AVRII and KPNI-HF, we cut GFP-Gephyrinb (without an
340 ATG) from the pCS 2.1 backbone and inserted it in frame into p3E_p2A to generate p3E_p2A-
341 GFP-Gephyrinb-TGA-polyA.
342 *PSD-95/dlg4b* transcript NM_214728.1 encodes a protein that is 76% identical and 83%
343 similar to rat *Dlg4* (NP_062567.1), and was thus chosen for use in our studies. We added GFP to
344 the 3'end because N-terminal palmitoylation of PSD-95 is necessary for its synaptic localization,
345 and receptor clustering[34,35]. It was cloned from cDNA with primers (Supplementary Table 1)
346 similar to *gephyrin* as described above. We refer to PSD-95-3xGGGGS-GFP as PSD-95-GFP. We
347 generated pME_ATG-PSD-95-GFP-TAA and p3E_p2A-PSD-95-GFP-TGA-polyA.

348 pME_myrGFP and pME_myrTagRFP-T were generated using PCR and BP reaction, using
349 Fyn myristoylation and palmitoylation domain. pGP-CMV-GCaMP6s (Addgene 40753) was used
350 as a template and 3 primers were used in a Q5 PCR (15 cycles at 71° C and 20 cycles at 72° C) to
351 amplify GCaMP6s and add Kozak sequence, myr (Fyn myristoylation and palmitoylation
352 domain), attB1, and attB2 sequences. This PCR product was used to generate
353 pME_myrGCaMP6s-TAA using BP reaction.
354 We obtained multiple plasmids from Tol2 kits: pDestTol2pA2, pDONR221, p5E_10xUAS,
355 p3E_polyA, p3E_p2A[36], p5E_sox10$_{7.2kb}$[31], pDestTol2pACryGFP (pDestTol2GE),
356 pDestTol2pACrymCherry (pDestTol2RE).
357 Using Gateway LR reactions (Invitrogen 11791020), we generated the following
358 constructs: PA2-10xUAS:myrEGFP-PolyA, GE-10xUAS:myrGCaMP6s-TAA-polyA, PA2-
359 olig1:myrGCaMP6s-TAA-polyA, GE-10xUAS:GFP-Gephyrinb-TAA-polyA, RE-10xUAS:GFP-
360 Gephyrina-TAA-polyA, GE-10xUAS:PSD-95-GFP-TAA-polyA, PA2-sox10:myrTagRFP-T-P2A-GFP-
361 Gephyrinb-polyA, PA2-sox10:myrTagRFP-T-P2A-PSD95-GFP-polyA. We used Mnx1:Gal4[37] to
362 drive myrGCaMP6s expression in motor neurons. We used Huc-Kalta4[31], UAS:TeTxLc-
363 tdtomato[21] to drive TeTxLc expression in neurons. All constructs generated in this study were
364 fully sequenced (except *sox10* and *olig1* promoters).
365 ***Cell specific CRISPR/Cas9 plasmid construction and CRISPR/Cas9-mediated gene disruption***
366 We used 5xUAS-hsp70promoter-Cas9-T2A-GFP, U6:sgRNA1;U6:sgRNA2[38] (Addgene 74009) as a
367 backbone and performed the following modifications: replacement of the 5xUAS-hsp70
368 promoter with the 10xUAS-E1b-bactin-Kozak promoter because we found the original promoter
369 expressed in many non-specific cell types when injected into *Tg(sox10:Kalta4)*; replacement of

370 T2A-GFP with myrmScarletI-p2A and added to the 5'end of Cas9; addition of polyA to the 3' end
371 of Cas9. Four sets of primers and 2 previously made plasmids (Tol2-10xUAS-E1b-mScarletI and
372 Tol2-10xUAS:cas9-P2A-TagRFPTcaax) were used to generate 4 segments. These segments were
373 integrated into the backbone by NEBuilder HiFi assembly (NEB E2621S). The new construct is
374 referred to as 10xUAS:myrmScarletI-p2A-Cas9, U6:sgRNA1;U6:sgRNA2.
375 CHOPCHOP and Crisprscan were used to identify 2 sgRNA sequences for each gene of
376 interest: *gephyrina* exon 2, GGTCATGAACGAGATCTTTGAGG; *gephyrinb* exon 7,
377 GGAGAGCCGGCAGGATGAACTGG; *myrf* exon 3, GACCCAACGGCGGTGCACCCGGG; *myrf* exon 4,
378 GCTGGAGTCCGGAGGAGACTCGG; *nlgn3a* exon 1, GGTGTATGATGCTTGTCCGGGGG; *nlgn3a* exon
379 4, GCCTTGTGTACTTAACCGGCTGG; *nlgn3b* exon 1, GATGCGGGTCGCTGTTGCCACGG; *nlgn3b*
380 exon 3, GGTAGTGTGCTGGCCAGCTACGG. The cutting efficiencies of these sgRNAs were verified
381 (>95%) via enzyme digestion of the targeted locus PCR product (CRISPRtest primers,
382 Supplementary Table 1). F0 larvae with *gephyrina* and *gephyrinb* sgRNA injected together with
383 1 ng Cas9 protein were used to examine the specificity of the Gephyrin antibody. BsaI and
384 BsmBI were used to insert the sgRNA into 10xUAS:myrmScarletI-p2A-Cas9,
385 U6:sgRNA1;U6:sgRNA2. The plasmids were injected with Tol2 transposase mRNA to generate
386 transgenic fish. *Tg(10xUAS:myrmScarletI-p2A-Cas9, U6:myrf^{exon3};U6:myrf^{exon4})*,
387 *Tg(10xUAS:myrmScarletI-p2A-Cas9, U6:nlgn3a^{exon1};U6:nlgn3a^{exon4})*, and
388 *Tg(10xUAS:myrmScarletI-p2A-Cas9, U6:nlgn3b^{exon1};U6:nlgn3b^{ex34})* larvae with sparsely labeled
389 oligodendrocyte were examined for morphology and sheath characteristics.
390 *Tg(10xUAS:myrmScarletI-p2A-Cas9, U6:sgRNA1;U6:sgRNA2)* larvae were used as controls.
391 ***Sparse labeling and generation of transgenic lines***

392 Fertilized zebrafish eggs at the 1-cell stage were microinjected with 1 nL of an injection
393 solution containing 20 ng/µL plasmid DNA, 25 ng/µL Tol2 transposase mRNA, 0.02% phenol
394 red and 0.2M KCl. Injected F0 animals were either used for single-cell analysis or raised to
395 adulthood to generate transgenic lines. To generate *Tg(10xUAS:myrGFP)* and
396 *Tg(10xUAS:myrGCaMP6s)*, adult F0 animals were outcrossed with *Tg(sox10:Kalta4)* zebrafish,
397 and F1 progenies were screened for germline transmission of the fluorescent reporters. F1
398 animals were further outcrossed and maintained in the *nacre* background to establish stable
399 transgenic lines with single copy insertion.

400 ***Mounting larvae for in vivo imaging***

401 For all live imaging experiments except those utilizing myrGCaMP6s, larvae were anesthetized
402 with 0.16 mg/mL (600 µM) tricaine in embryo medium. The fish were mounted in 0.8% low
403 melting agarose (Sigma A9414) on a coverslip for morphology and sheath examination or in 1.5%
404 low melting agarose in a dish for time lapse imaging (hours). For myrGCaMP6s imaging, larvae
405 were immobilized with 0.5 mg/ml non-depolarizing acetylcholine receptor antagonist
406 mivacurium chloride (Abcam) and mounted in 1.5% low melting agarose in a dish.

407 ***Confocal microscopy***

408 All imaging was performed on an upright Zeiss LSM 980 confocal with Airyscan 2 in 4Y fast
409 mode. For fixed tissues, a 63x/1.4 NA oil objective was used, and for live imaging, a 20x/1.0 NA
410 water objective was used. All images were taken in Zeiss software. We used the following lasers:
411 488 nm for EGFP, myrGCaMP6s, and Alexa488; 561 nm for TagRFP, mScarletI, and Alexa594;
412 639 nm for Alexa647. Fixed tissue was imaged with 0.15 µm z spacing with 1.6x to 2.5x zoom.
413 For *in vivo* analyses, PSD-95-GFP and GFP-Gephyrin were imaged with 2 µm z-spacing at an

414 interval of 5 min (for 30 min to 1 hour) or 20 min (for longer than 1 hour) at a zoom between
415 3.7x-10x depending on OPC cell size. myrGCaMP6s was imaged with 2 µm z-spacing at 0.5 Hz (4
416 planes scanned) for 10 min or 20 min (drug injection experiments) as previously described[4,12].
417 Images acquired at 0.5 Hz were analyzed along with images acquired at 10 Hz with a single
418 plane. No major differences were found on the Ca^{2+} spike characteristics, but 0.5 Hz acquisition
419 allows inclusion of more stacks and increases the number of events detected. Therefore, 0.5 Hz
420 was used throughout the study.

421 ***Drug delivery through ventricle injection***

422 For myrGCaMP6s experiments involving drug delivery, we injected drugs via ventricle injection
423 as described previously[12]. Briefly, following 10 min GCaMP6s imaging, a 1 nL mixture containing
424 0.2M KCL, 0.5% Dextran Texas Red 3000 MW (Thermo), and molecular biology grade H_2O
425 (control), TTX (0.5 mM), IEM-1460 (20 mM), AP5 (30 mM), or cadmium (100 mM) (all drugs
426 were kind gifts from Henrique von Gersdorff's lab) were pressure injected into the hindbrain
427 ventricle using an ASI MPPI-3. Between 15 and 35 min after injection, Dextran was imaged,
428 followed by another 10 min of GCaMP6s imaging. Dextran surrounding the imaged OPCs was
429 used to verify the drug delivery. TTX, IEM1460, AP5, and cadmium all caused fish paralysis,
430 further verifying efficient delivery of active drugs. After imaging, fish were removed from
431 mounting media. Larvae injected with control solution recovered full swimming activity within 3
432 minutes, and drug-injected paralyzed larvae maintained normal heartbeats for at least 3 hours.

433 ***Quantification and image analysis***

434 *OPC labeling during development*

435 We used *sox10* and *olig1* to label OPCs. *sox10* drives expression in both OPCs and myelinating
436 oligodendrocytes while *olig1* labels only OPCs. OPCs and myelinating oligodendrocytes can be
437 distinguished by cell morphology: OPCs only possess processes and myelinating
438 oligodendrocytes possess sheaths. Animal ages and corresponding OPC activity: 55-60 hpf
439 (hours post-fertilization, when OPCs are born, and migrate), 3 dpf (when OPCs initiate
440 differentiation), 5-14 dpf (when many OPCs complete differentiation.)

441 *Alignment rate and colocalization ratio*

442 Images of fixed tissue were analyzed in Imaris. "Surface" function was used to create a cell
443 surface and "Spot" function was used to generate $Spot_{PSS\ puncta}$. Then the cell surface was used
444 as a mask to generate $Spot_{PSS\ puncta\ in\ OPCs}$, which was further verified by crosschecking its overlap
445 with $Spot_{PSS\ puncta}$. $Spot_{PSS\ puncta\ in\ OPCs}$ was analyzed for puncta number or density. To examine the
446 alignment of MAGUK (Gephyrin) and Synapsin, we used "Spot" function to generate $Spot_{Synapsin}$
447 $_{puncta}$. By determining the proximity $Spot_{PSS\ puncta\ in\ OPCs}$ to $Spot_{Synapsin\ puncta}$ using MATLAB-enabled
448 "Colocalize Spots" function (<0.1 µm), we could identify PSSs in OPCs that align with Synapsin
449 and calculate the alignment rate. To calculate the colocalization ratio of MAGUK (Gephyrin)-
450 Synapsin, we used the Imaris "Coloc" function to generate a new M&S coloc channel based on
451 the overlapping pixels between MAGUK (Gephyrin) and Synapsin channel above thresholds.
452 "Surface" function was used to generate M&S coloc surface of the whole section, MAGUK
453 (Gephyrin) (M) surface of the whole section, and OPC surface. OPC surface was used as a mask
454 to generate masked M&S coloc channel and MAGUK (Gephyrin) channel. These masked
455 channels were then used to generate M&S coloc surface in OPCs and M surface in OPCs." The
456 colocalization ratio in OPCs and neurons was calculated as follows:

457 $$\boldsymbol{Colocalization\ ratio_{OPCs}} = \frac{\boldsymbol{Volume_{M\&S\ coloc\ surface\ in\ OPCs}}}{\boldsymbol{Volume_{M\ surface\ in\ OPCs}}};$$

458 $$\boldsymbol{Colocalization\ ratio_{neurons}} =$$

459 $$\frac{\boldsymbol{Volume_{M\&S\ coloc\ surface\ of\ the\ whole\ section} - Volume_{M\&S\ coloc\ surface\ in\ OPCs}}}{\boldsymbol{Volume_{M\ surface\ of\ the\ whole\ section} - Volume_{M\ Surface\ in\ OPCs}}}.$$

460 *PSS puncta identification and analysis*

461 Live Images of PSD-95-GFP and GFP-Gephyrin were processed in ImageJ and synaptic puncta
462 were identified and tracked with Trackmate[39]. The images were first maximum projected and
463 stabilized using "Image Stabilizer." In Trackmate, parameters were set as follows: LOG mode,
464 diameter 0.75 µm, Quality>100, contrast>0.19 and signal noise >0.35, LAP linking with 0.5 µm
465 distance and 2 max gap frames allowed were applied. The identified puncta at each frame were
466 then manually examined to remove poor quality tracks. Neighboring puncta may sometimes be
467 incorrectly linked between timelapses; therefore, manual examinations were done to fix these
468 link errors. The data output was analyzed in MATLAB with custom scripts to calculate puncta
469 number per cell at each timepoint, puncta duration and diameter. Heatmaps of puncta over
470 time were generated using the output data with Heatscatter
471 (https://www.mathworks.com/matlabcentral/fileexchange/47165-heatscatter-plot-for-
472 variables-x-and-y). To generate figures of mean and standard deviation as shade, we used a
473 modified script (https://www.mathworks.com/matlabcentral/fileexchange/29534-stdshade).
474 To analyze the puncta number during OPC differentiation, time points when OPC shows first
475 sheath (differentiation) and when myelinating oligodendrocyte's last process disappeared and
476 all process transformed into sheaths (maturation) were noted for each cell. In MATLAB, this
477 information is used to divide the puncta number into before and after differentiation or

478 maturation for each cell. The traces were generated after the data was realigned to set the
479 timepoint of differentiation or maturation as time 0.

480 *Ca^{2+} events analysis*

481 myrGCaMP6s images of z-stacks were maximum projected and stabilized using "Image
482 Stabilizer." The images were assigned with random names using "blindr"
483 (https://github.com/U8NWXD/blindr) before analysis and reassigned with the original names
484 after analysis. The regions of Ca^{2+} events (ROI) were identified by "GECIquant"[40] first and then
485 manually examined frame by frame. The intensity and area of each ROI were exported and
486 processed in MATLAB through custom scripts. Briefly, $\Delta F/F_{average}$ ($\Delta F=F- F_{average}$) was calculated
487 to generate traces and to identify intensity peaks using "findpeaks" in MATLAB with filtering
488 parameters (3 standard deviations above average, prominence larger than 40% of the baseline,
489 and peak area larger than 2.5). Rare elevated Ca^{2+} signal for extended periods of time (longer
490 than 50 seconds) were excluded. Peaks were manually verified against the image. Several Ca^{2+}
491 characteristics were measured: peak amplitude, peak duration, Ca^{2+} microdomain number, Ca^{2+}
492 microdomain area, and frequency of Ca^{2+} activity. A region with multiple OPCs was analyzed for
493 TeTxLc experiment, while single OPC was analyzed for the rest of experiments. To examine the
494 proximity of synaptophysin-TagRFP to Ca^{2+} microdomain, Ca^{2+} microdomains were identified as
495 above, and their locations were first compared to synaptophysin-TagRFP manually plane by
496 plane and then verified by Imaris. In Imaris, using "Spot" function and "Surface" function, we
497 generated synaptophysin-TagRFP puncta and OPC surface, with which we identified the puncta
498 that were close to OPC surfaces using a MATLAB-enabled "Spot-to-Surface" function (0.1 µm

499 threshold). These puncta were manually checked against Ca^{2+} microdomains identified through

500 morphological landmarks in Imaris.

501 *Oligodendrocyte and myelin sheath analysis*

502 To analyze myelin sheath length and number, we used ImageJ ROI manager to trace all sheaths

503 of sparsely labeled oligodendrocytes between segments 1 and 15 in spinal cord. The number of

504 oligodendrocytes analyzed per fish was limited to 3 to ensure even weight among individual fish.

505 Sheath traces and the corresponding images were blinded using "Blind analysis encrypter." The

506 sheath length and number were then analyzed in MATLAB with custom scripts and matched

507 with the original genotype following analysis.

508 ***Statistics***

509 Data are shown as mean±SEM., with individual data points shown as circles. We conducted

510 Shapiro-Wilk's test and Levene's test to verify data normality and homoscedasticity,

511 respectively, before performing two-sided *t*-test for unpaired groups, paired *t*-test for paired

512 groups, and one-way ANOVA and Tukey's test for more than 3 groups. If the data did not pass

513 normality tests, we used Kruskal-Wallis test for more than 3 groups. These analyses were

514 performed either in GraphPad Prism or MATLAB. The significance and statistical analyses

515 employed were indicated in figure legends. Animal and cell number used for each experiment,

516 t-values and df for *t*-tests, and *F* values and df for ANOVA were indicated in either figure

517 legends or Supplemental Table 2. Data collection was not performed blindly due to the

518 experimental conditions, but analyses were performed blindly as indicated. Sample size was

519 chosen based on standard deviation and effect (http://www.biomath.info/power/ttest.htm).

520 Sex is not yet determined in zebrafish at the ages employed in our study and so cannot be
521 considered as a biological variable.
522
523 **Reporting summary**
524 Further information on research design is available in the Nature Research Reporting Summary
525 linked to this manuscript.
526
527 **Data availability**
528 All research materials are available upon request. Source data are provided with this paper.
529
530 **Code availability**
531 All custom scripts are available upon request.
532
533 31. Almeida, R. G. & Lyons, D. A. Intersectional gene expression in zebrafish using the split
534 KalTA4 system. *Zebrafish* **12**, 377–386 (2015).
535 32. Fuhrmann, J. C. *et al.* Gephyrin interacts with dynein light chains 1 and 2, components of
536 motor protein complexes. *J. Neurosci.* **22**, 5393–5402 (2002).
537 33. Smolinsky, B., Eichler, S. A., Buchmeier, S., Meier, J. C. & Schwarz, G. Splice-specific
538 functions of gephyrin in molybdenum cofactor biosynthesis. *J. Biol. Chem.* **283**, 17370–
539 17379 (2008).
540 34. Craven, S. E., El-Husseini, A. E. & Bredt, D. S. Synaptic targeting of the postsynaptic
541 density protein PSD-95 mediated by lipid and protein motifs. *Neuron* **22**, 497–509 (1999).

542 35. Topinka, J. R. & Bredt, D. S. N-terminal palmitoylation of PSD-95 regulates association
543 with cell membranes and interaction with K+ channel K(v)1.4. *Neuron* **20**, 125–134 (1998).
544 36. Kwan, K. M. *et al.* The Tol2kit: A multisite gateway-based construction Kit for Tol2
545 transposon transgenesis constructs. *Dev. Dyn.* **236**, 3088–3099 (2007).
546 37. Wyart, C. *et al.* Optogenetic dissection of a behavioural module in the vertebrate spinal
547 cord. *Nature* **461**, 407–410 (2009).
548 38. Di Donato, V. *et al.* 2C-Cas9: A versatile tool for clonal analysis of gene function. *Genome*
549 *Res.* **26**, 681–692 (2016).
550 39. Tinevez, J. Y. *et al.* TrackMate: An open and extensible platform for single-particle
551 tracking. *Methods* **115**, 80–90 (2017).
552 40. Srinivasan, R. *et al.* Ca2+ signaling in astrocytes from Ip3r2 -/- mice in brain slices and
553 during startle responses in vivo. *Nat. Neurosci.* **18**, 708–717 (2015).
554

555 **Acknowledgments**

556 This work was supported by an NMSS postdoctoral fellowship and a Warren Alpert
557 Distinguished Scholar Award (JL) and NIH/NINDS grant 1R21NS120650 (KRM). We thank Dwight
558 Bergles and members of the Monk lab for discussions and critical reading of the manuscript. We
559 are indebted to Austin Forbes, Tia Perry, and Grace Halsell-Vore for fish care. We thank Rafael
560 Almeida, Paul Brehm, Marc Freeman, Henrique von Gersdorff, Eric Gouaux, David Lyons, Alex
561 Nechiporuk, and Teresa Nicolson for reagents and suggestions as well as Fernanda Coelho,
562 Stefanie Kaech Petrie and OHSU microscopy core staff for feedback and assistance in imaging.
563 We thank Lori Vaskalis for graphic design.

564

565 **Author Contributions**

566 J.L. and K.R.M. conceived the project. J.L. carried out experiments and data analyses. T.M.

567 generated constructs for *nlgn3a* and *nlg3b* disruption. T.C. provided key resources prior to their

568 publication. J.L. and K.R.M wrote the manuscript, and all authors edited the manuscript.

569

570 **Competing interests**

571 The authors declare no competing interests.

572

573 **Additional information**

574 **Supplementary Information** is available for this paper.

575 **Correspondence and requests for materials** should be addressed to Jiaxing Li or Kelly Monk.

576

577

578

579

580

581

582

583

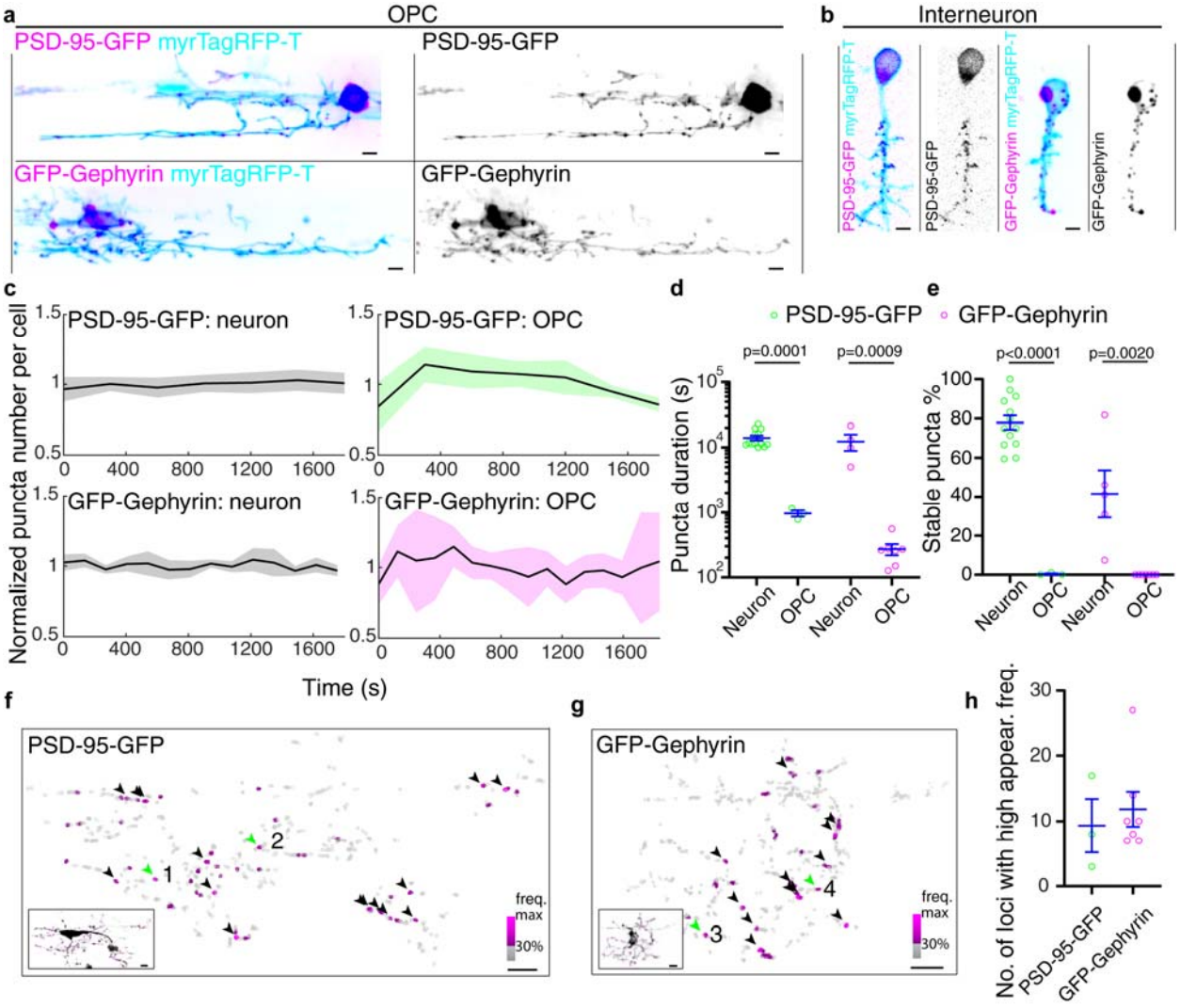

Figure 1. PSD-95-GFP and GFP-Gephyrin imaging reveals dynamic synapses that assemble at specific locations in OPCs in vivo. **a**-**b**, Representative images of PSD-95-GFP and GFP-Gephyrin (magenta) in spinal cord (**a**) OPCs and (**b**) neurons at 3 dpf. Cell membranes indicated with cyan. **c**, Quantification of puncta number per cell within 30 minutes for PSD-95-GFP and GFP-Gephyrin in neurons and OPCs, normalized to the average. Black line, average; shaded area, sd. **d**-**e**, Quantification of PSD-95-GFP (green) and GFP-Gephyrin (magenta) (**d**) puncta duration in log scale and (**e**) % of stable puncta that lasts over 10,000 seconds in neurons and OPCs at 3 dpf. From left, n = 13, 3, 5 and 7 cells, from 6, 3, 4 and 4 fish. **f**,**g**, Heatmaps of puncta appearance frequency over time for (**f**) PSD-95-GFP and (**g**) GFP-Gephyrin. 30% of max frequency is used as coloring threshold: below threshold, grey; above threshold, a shade of magenta corresponding to the frequency. Loci with high puncta appearance frequency (> 3 sd above average) are marked with arrowheads. The numbers with green arrowheads indicate puncta shown in time lapse images in Extended Data Fig. 2c-d. Bottom left, snapshots of OPCs with puncta marked with magenta circles. **h**, Quantification of loci with high puncta appearance frequency in OPCs. From left, n = 3 and 7 cells from 3 and 5 fish. All data are represented as mean ± SEM; unpaired *t*-test; Scale bar, 5 µm.

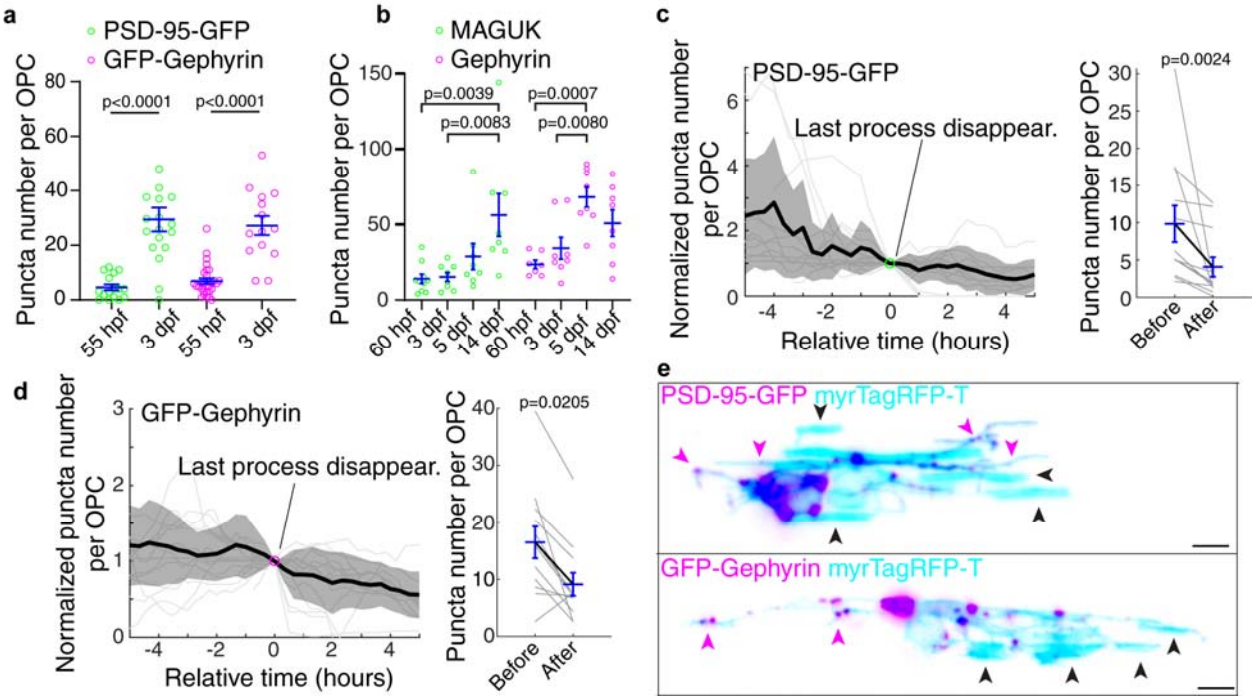

Figure 2. PSSs in OPCs are developmentally regulated. **a**, Quantification of PSD-95-GFP (green) and GFP-Gephyrin (magenta) puncta number per cell in the spinal cord at 55 hpf and 3 dpf by *in vivo* imaging. **b**, Quantification of MAGUK (green) and Gephyrin (magenta) puncta number per cell in spinal cord at different ages by IHC. **c**-**d**, Quantification of (**c**) PSD-95-GFP and (**d**) GFP-Gephyrin puncta number in OPCs before and after the last process disappearance, which is set as time zero. Left, traces show the average (black line) and the sd (shade) with individual traces (grey line). Right, paired comparison before and after time zero. **c**, n= 12 cells from 8 fish; **d**, n= 12 cells from 8 fish. **e**, Representative images of PSD-95-GFP and GFP-Gephyrin (magenta) in differentiating oligodendrocytes (cyan) at 55-60 hpf. All data are represented as mean ± SEM; N.S., not significant; (**a**) unpaired *t*-test, (**b**) one-way ANOVA followed by Tukey's test, and (**c**-**d**) ratio-paired *t*-test; scale bar 5 µm.

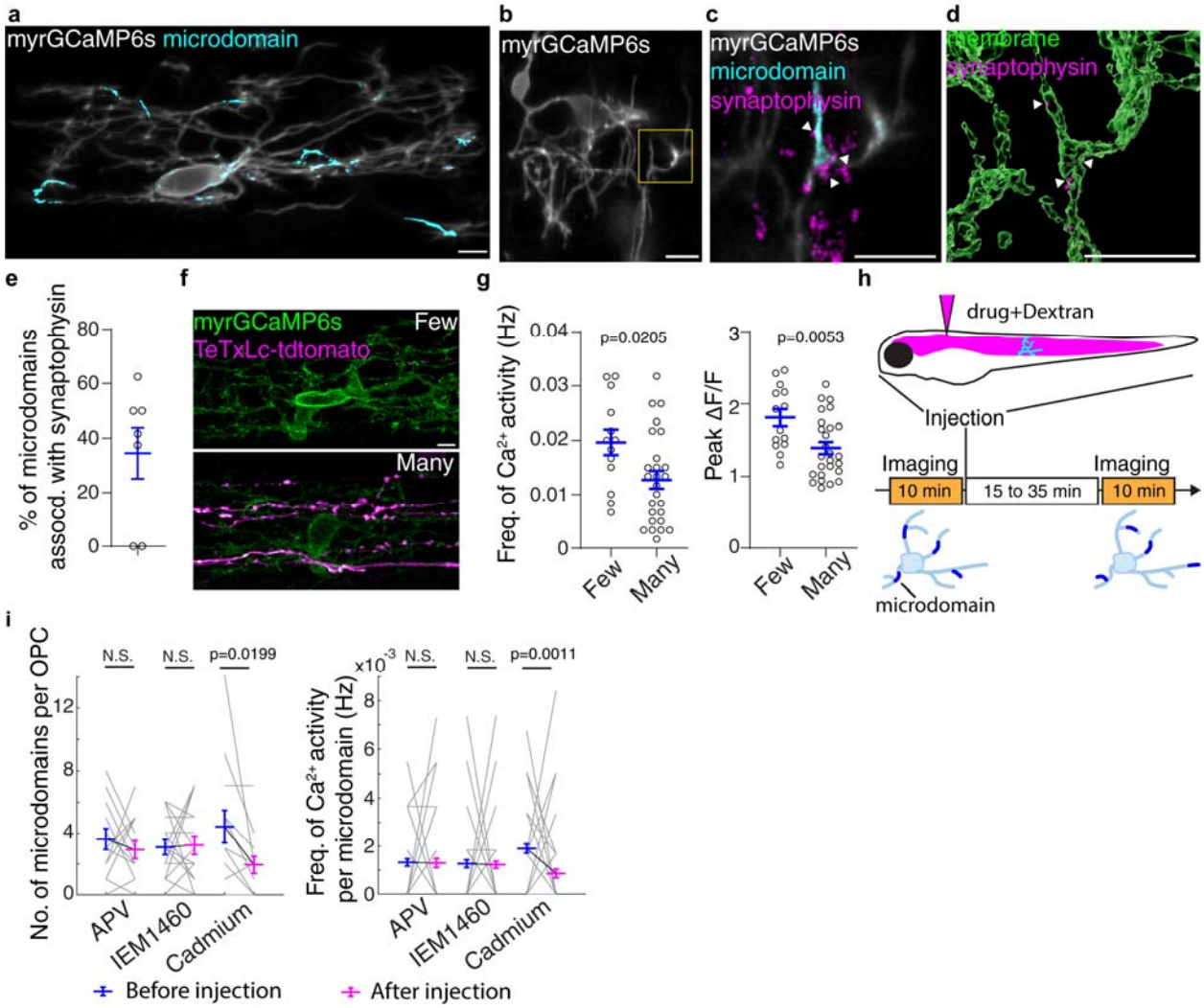

Figure 3. Synapses and VGCCs, but not NMDA or CP-AMPA receptors, contribute to generating intrinsic OPC Ca^{2+} activity in vivo. **a**, Representative images of plasma membrane-targeting myrGCaMP6s in an OPC (grey) showing activity in microdomains (cyan). **b**-**c**, Representative images of (**b**) an OPC (grey) visualized by myrGCaMP6s showing (**c**) proximity between an microdomain with Ca^{2+} activity (cyan) and presynaptic synaptophysin-tagRFP (magenta). **d**, 3-D reconstruction showing synaptophysin-tagRFP puncta (magenta) that are within 0.1 µm from the OPC surface (arrowheads). **e**, Quantification of the percentage of Ca^{2+} microdomains that are associated with synaptophysin-tagRFP (n = 7 cells from 7 fish). **f**, Representative images of OPCs neighboring few (<4) and many (≥4) axons expressing *TeTxLc-tdtomato*. **g**, Quantification of frequency of Ca^{2+} activity and peak amplitude in OPCs that neighbor few (<4) or many (≥4) TeTxLc-expressing axons at 5 dpf. From left, n = 14 and 26 cells from 8 and 15 fish. **h**, Schematic of hindbrain ventricle injection. **i**, Quantification of Ca^{2+} microdomain number per OPC and frequency of Ca^{2+} activity per microdomain in OPCs before (blue) and after (magenta) injection of 1 nL of AP5 (30 mM), Cadmium (100 mM), or IEM1460 (20 mM) solution at 5 dpf. Paired data indicated with grey line. From left, n = 13, 16 and 13 cells from 7, 7 and 7 fish. All data are represented as mean ± SEM; N.S., not significant; (**g**) unpaired *t*-test or (**i**) paired *t*-test; scale bar 5 µm.

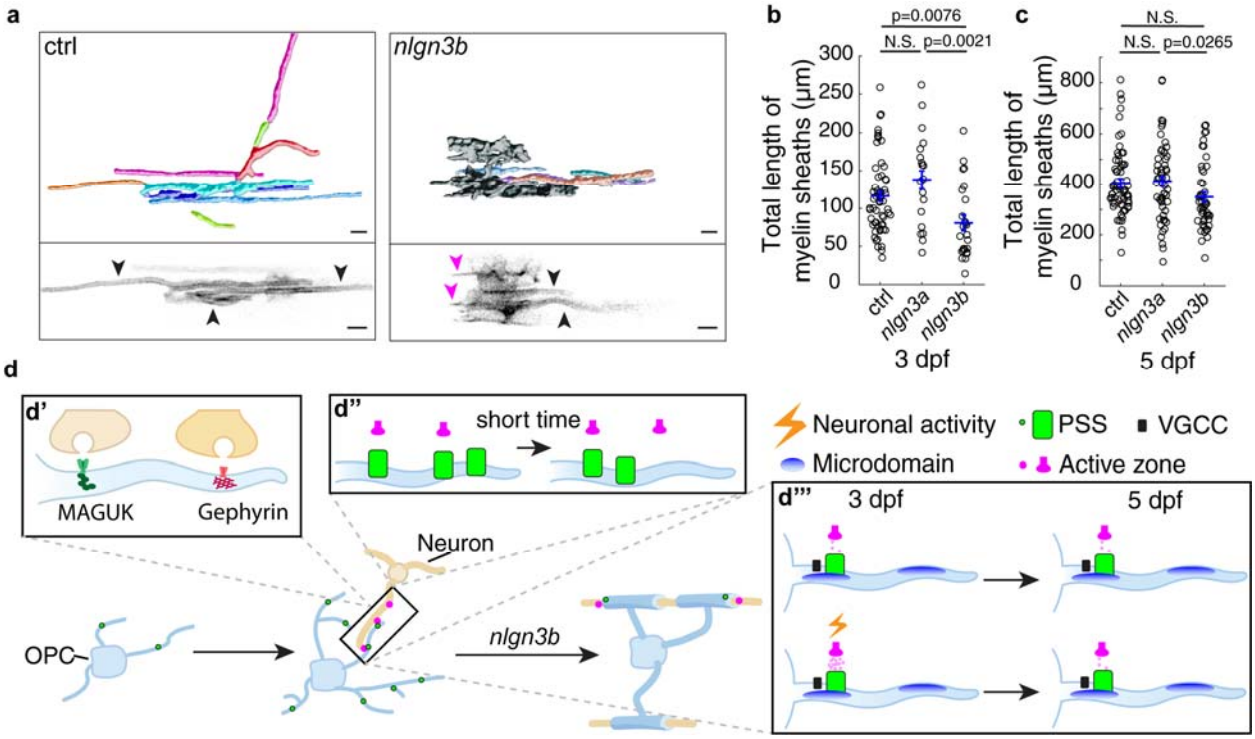

Figure 4. Synaptic component nlgn3b is important for oligodendrocyte differentiation and myelination. **a**, Morphology of control (ctrl), and *nlgn3b*-targeted myelinating oligodendrocytes at 5 dpf. Top, 3D-reconstructed single oligodendrocyte with sheath (colored) and non-sheath (white). Bottom, single plane with sheath (black arrowheads) and processes (magenta arrowheads). **b**-**c**, Quantification of total length of myelin sheaths of myelinating OLs at (**b**) 3 dpf and (**c**) 5 dpf in ctrl, *nlgn3a*-, and *nlgn3b*-targeted fish. From left, 3 dpf, n = 61, 19 and 25 cells from 18, 14 and 18 fish; 5 dpf, n = 66, 56 and 47 cells from 24, 36 and 30 fish. All data are represented as mean ± SEM; N.S., not significant; (**b**,**c**) Kruskal-Wallis test; scale bar 5 µm. **d**, Schematic model: **d'**, synapses containing MAGUK (green) and Gephyrin (red) form between neurons and OPCs; PSSs in OPCs (green with black border) increase in number through development and decrease upon differentiation, while disruption of synaptic gene *nlgn3b* impairs OPC differentiation; **d''**, PSSs in OPCs are dynamic with frequent assembly, and many of them do not align with presynaptic active zone (magenta); **d'''**, Neuron-OPC synapses are in proximity to some Ca^{2+} microdomains (blue), and, together with VGCCs (Black), contribute to generating intrinsic OPC Ca^{2+} activity. Evoked synaptic release contributes to intrinsic OPC Ca^{2+} activity at 3 dpf but not 5 dpf.

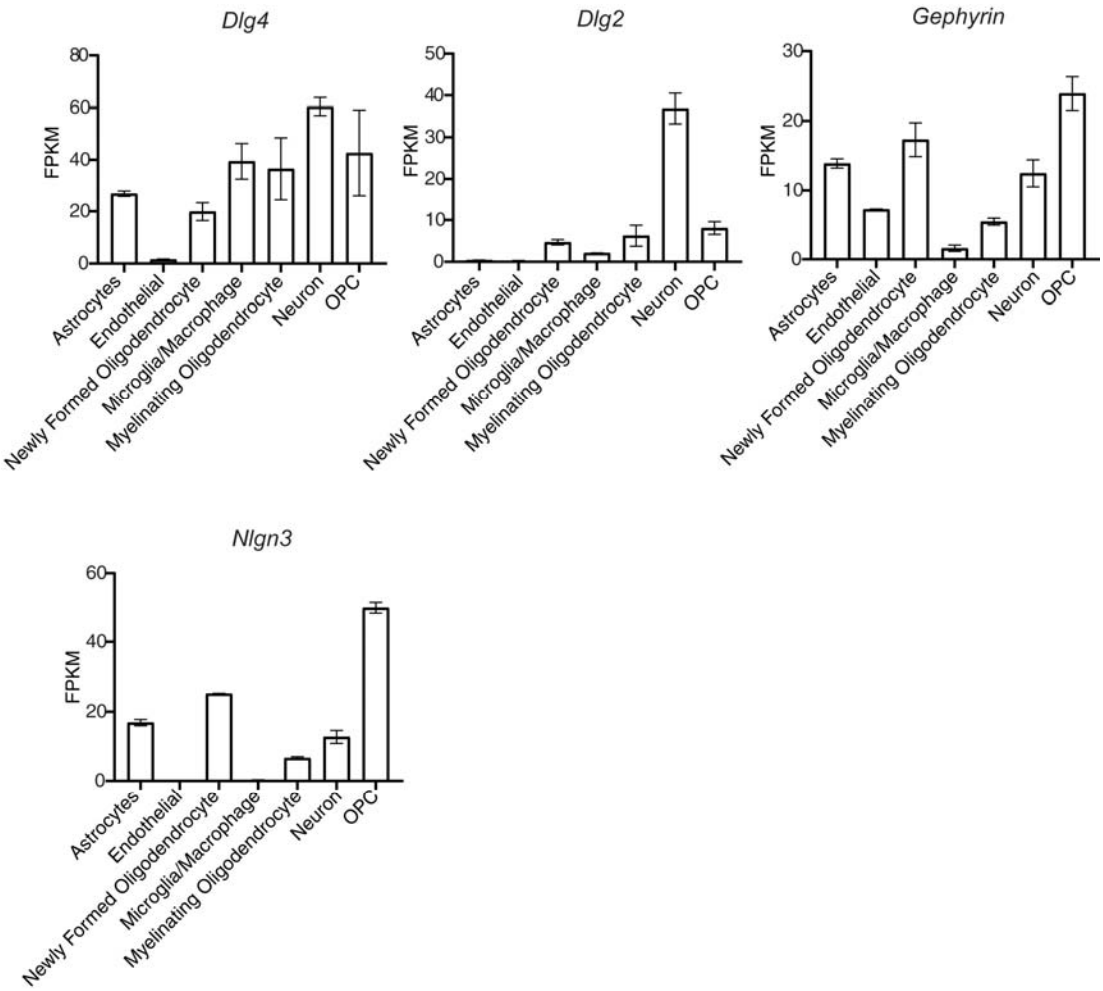

Extended Data Figure 1. PSD-95 (dlg4), PSD-93 (dlg2), gephyrin, and nlgn3 are expressed in OPCs. Summary of RNA-seq expression reported of mammalian *Dlg4 (MAGUK)*, *Dlg2 (MAGUK)*, *Gephyrin*, and *Nlgn3* in different CNS cell types[26].

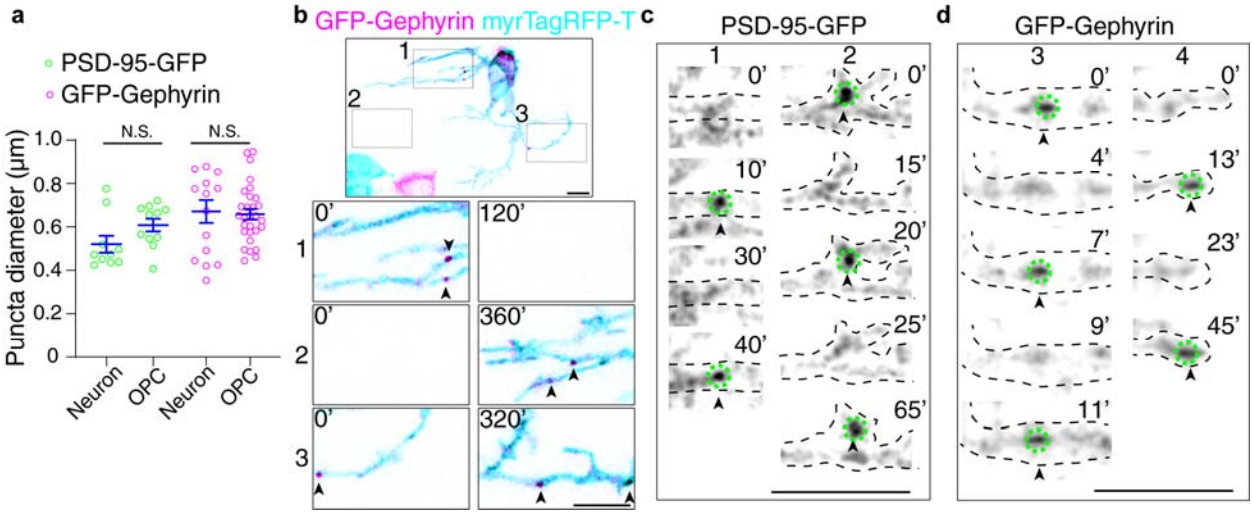

Extended Data Figure 2. in vivo analysis of PSSs. **a**, Quantification of PSD-95-GFP (green) and GFP-Gephyrin (magenta) puncta diameter in neurons and OPCs at 2-3 dpf in the spinal cord. From left, n = 10, 11, 15 and 29 cells from at least 8 fish. **b**, Representative images of GFP-Gephyrin (magenta) as an OPC remodels its processes (cyan) at 3 dpf. 3 enlarged regions were shown at different time points (minutes) and puncta were indicated with arrowheads. **c**-**d**, Representative time-lapse images of (**c**) PSD-95-GFP and (**d**) GFP-Gephyrin within OPC processes. The numbers indicate the corresponding puncta in **Fig. 1f**,**g**. Puncta 1 and 3 are in stable processes; puncta 2 and 4 are in dynamic processes. The dashed lines outline the process, and arrowheads indicate puncta appearance. Time unit is in minutes. All data are represented as mean ± SEM; (**a**) unpaired *t*-test. Scale bar 5 µm.

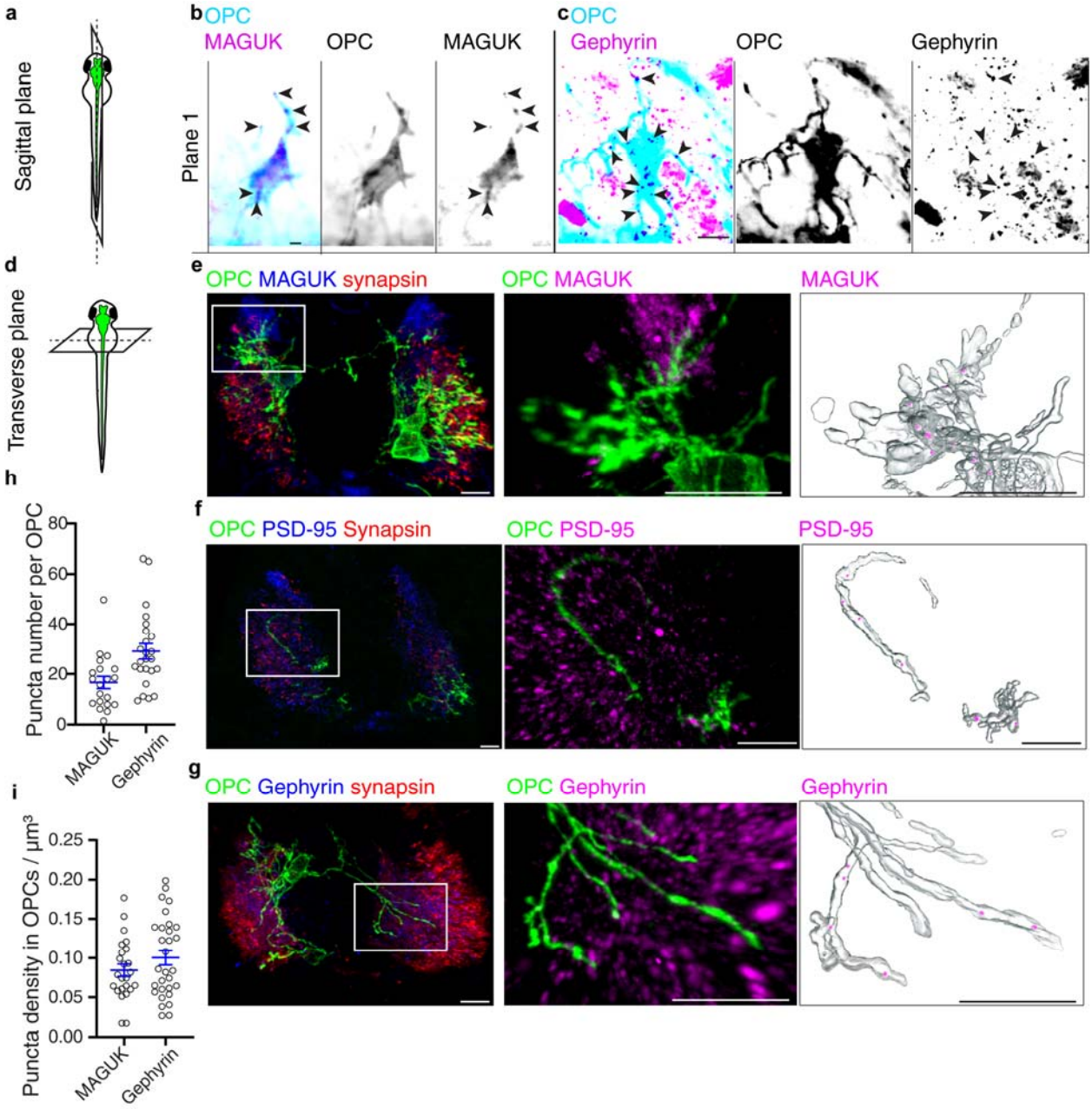

Extended Data Figure 3. Postsynaptic organizers, MAGUK, PSD-95, and Gephyrin, are present in zebrafish spinal cord OPCs. **a**, Schematic fish model showing sagittal planes. **b**-**c**, Two representative single-sagittal-plane IHC images showing (**b**) MAGUK and (**c**) Gephyrin within OPCs in *Tg(sox10:GFP-caax)* spinal cord at 3 dpf. OPCs identified by GFP and shown in cyan. Arrowheads indicate PSS puncta. The color was inverted to optimize visualization. **d**, Schematic fish model showing the transverse planes. **e**-**g**, Representative images of (**e**) MAGUK, (**f**) PSD-95 and (**g**) Gephyrin staining in *Tg(olig1:Kalta4,10xUAS:myrGFP)* spinal cord at 3 dpf. From left, spinal cord sections, enlarged images, and 3D-reconstructed images to reveal OPC surface and PSS puncta (magenta sphere). **h**-**i**, Quantification of MAGUK and Gephyrin (**g**) puncta number in OPCs and (**h**) puncta density in OPCs. **h**, n= = 20 and 24 cells from 9 and 10 fish; **i**, n = 24 and 30 cells from 9 and 10 fish. All data are represented as mean ± SEM; unpaired *t*-test; scale bar 5 µm.

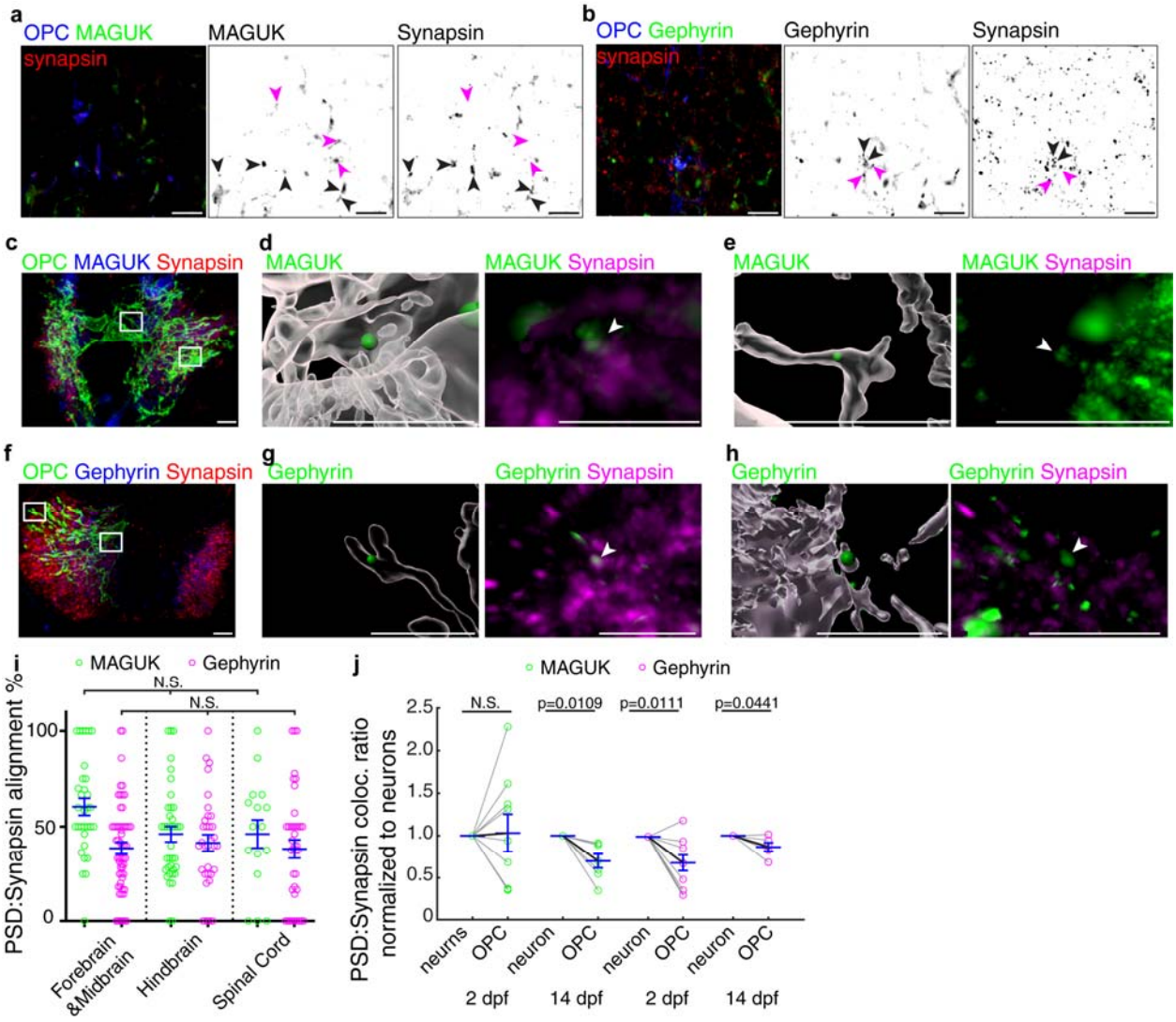

Extended Data Figure 4. Many but not all PSS puncta in OPCs align with presynaptic structures. **a**-**b**, Representative single-sagittal-plane IHC images showing (**a**) MAGUK and (**b**) Gephyrin with presynaptic marker Synapsin in *Tg(sox10:GFP-caax)* spinal cord at 3 dpf. From left, merged channels, MAGUK or Gephyrin channel, and Synapsin channels. Black arrowheads indicate the alignment of postsynaptic puncta with presynaptic Synapsin. Magenta arrowheads point to postsynaptic puncta in OPCs that do not align with presynaptic Synapsin. **c**-**h**, Representative transverse IHC images of Synapsin and (**c**-**e**) MAGUK or (**f**-**h**) Gephyrin staining in *Tg(olig1:Kalta4,10xUAS:myrGFP)* spinal cord OPCs at 3 dpf. From left, (**c**,**f**) spinal cord sections and zoomed-in 3D reconstructed images to reveal PSS puncta (green sphere) (**d**,**g**) that align with presynaptic puncta, and (**e**,**h**) that do not. The arrowheads indicate the PSS puncta. **i**, The % of MAGUK and gephyrin puncta on OPC processes that align with presynaptic Synapsin in forebrain & midbrain, hindbrain, and spinal cord at 3 dpf. From left, n= 32, 57, 38, 33, 16 and 39 cells from at least 10 fish. **j**, Quantification of MAGUK (green) and Gephyrin (magenta) colocalization ratio with Synapsin in OPCs, normalized to the colocalization ratio in neurons at 2 dpf and 14 dpf. From left, n = 9, 7, 9 and 7 fish. All data are represented as mean ± SEM; N.S., not significant; (**i**) one-way ANOVA followed by Tukey's test or (**j**) paired *t*-test; Scale bar 5 µm.

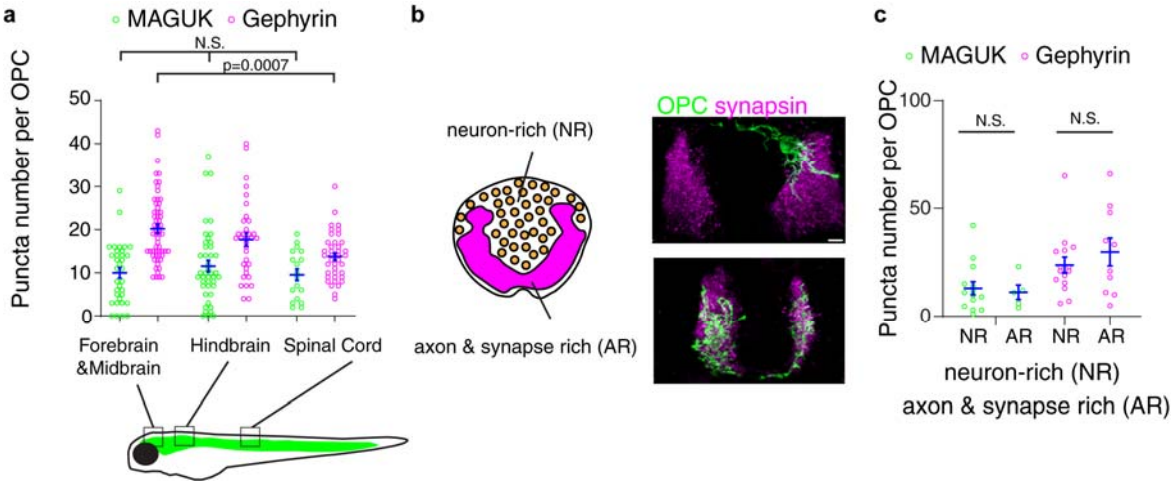

692

693 ***Extended Data Figure 5. PSS numbers in OPCs show few regional and no subgroup differences.*** **a**,
694 Quantification of MAGUK (green) and Gephyrin (magenta) puncta number per OPC at 3 dpf across the
695 CNS regions indicated by the schematic: forebrain & midbrain, hindbrain, and spinal cord. From left, n =
696 34, 59, 43, 34, 18 and 40 cells from at least 10 fish. **b**, Schematic model showing the neuron-rich (NR)
697 and axon & synapse-rich (AR) regions and two representative images showing OPCs with soma localized
698 to NR (top) and AR (bottom) regions in *Tg(olig1:Kalta4,10xUAS:myrGFP)* spinal cord. **c**, Quantification of
699 MAGUK (green) and Gephyrin (magenta) puncta number per cell between OPCs with their soma
700 localized to NR and AR regions at 2-3 dpf. From left, n = 14, 5, 15 and 10 cells from at least 5 fish. All data
701 are represented as mean ± SEM; N.S., not significant; (**a**) one-way ANOVA followed by Tukey's test and
702 (**c**) unpaired *t*-test; scale bar 5 µm.
703

704

705

706

707

708

709

710

711

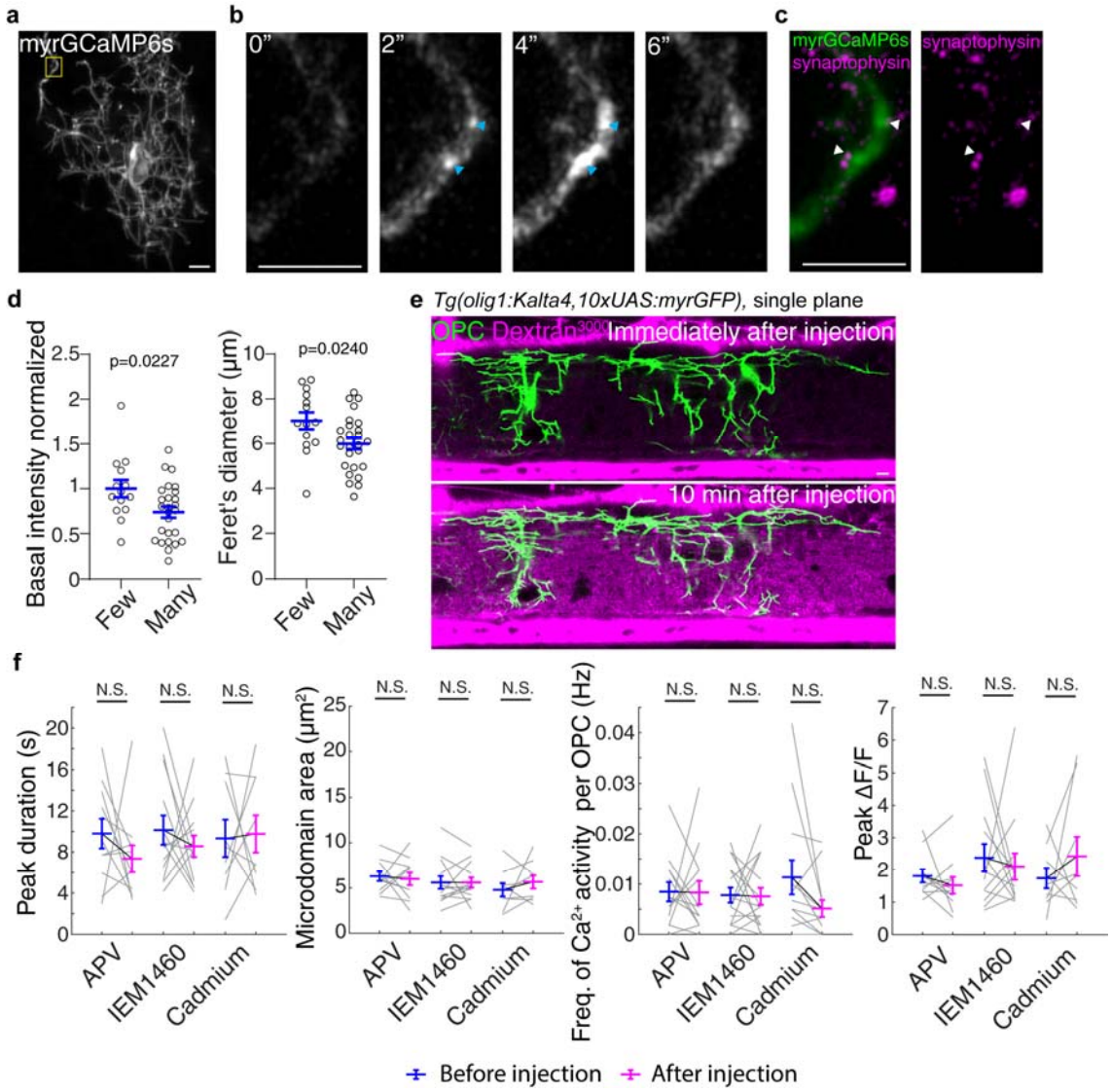

712

713 ***Extended Data Figure 6. Synapses contribute to generating intrinsic OPC Ca^{2+} activity in vivo.*** **a**, An OPC
714 visualized by myrGCaMP6s. **b**, In the enlarged region from (**a**), two Ca^{2+} spikes initiate as puncta and
715 then spread to form microdomains, indicated by blue arrowheads. The time is in seconds. **c**, The two
716 microdomains from (**b**) were in proximity (within 0.1 µm) with presynaptic synaptophysin-tagRFP
717 (magenta), indicated by white arrowheads. **d**, Quantification of basal intensity and Feret's diameter in
718 OPCs that neighbor few (< 4) or many (≥ 4) TeTxLc-expressing axons at 5 dpf. From left, n = 14 and 26
719 cells from 8 and 15 fish. **e**, Representative single-plane images of individual spinal cord OPCs
720 immediately and 10 min after hindbrain ventricle injection of dextran MW3000 Texas Red (magenta) in
721 *Tg(olig1:Kalta4,10xUAS:myrGFP)* larva. **f**, Quantification of peak duration and area of Ca^{2+} microdomains,
722 frequency of Ca^{2+} activity and peak amplitude before (blue) and after (magenta) APV, Cadmium, or
723 IEM1460 injection at 5 dpf. Data in pairs indicated with grey lines. From left, n = 13, 16 and 13 cells from
724 7, 7 and 7 fish. All data are represented as mean ± SEM; N.S., not significant; (**d**) unpaired *t*-test and (**f**)
725 paired *t*-test; scale bar 5 µm.

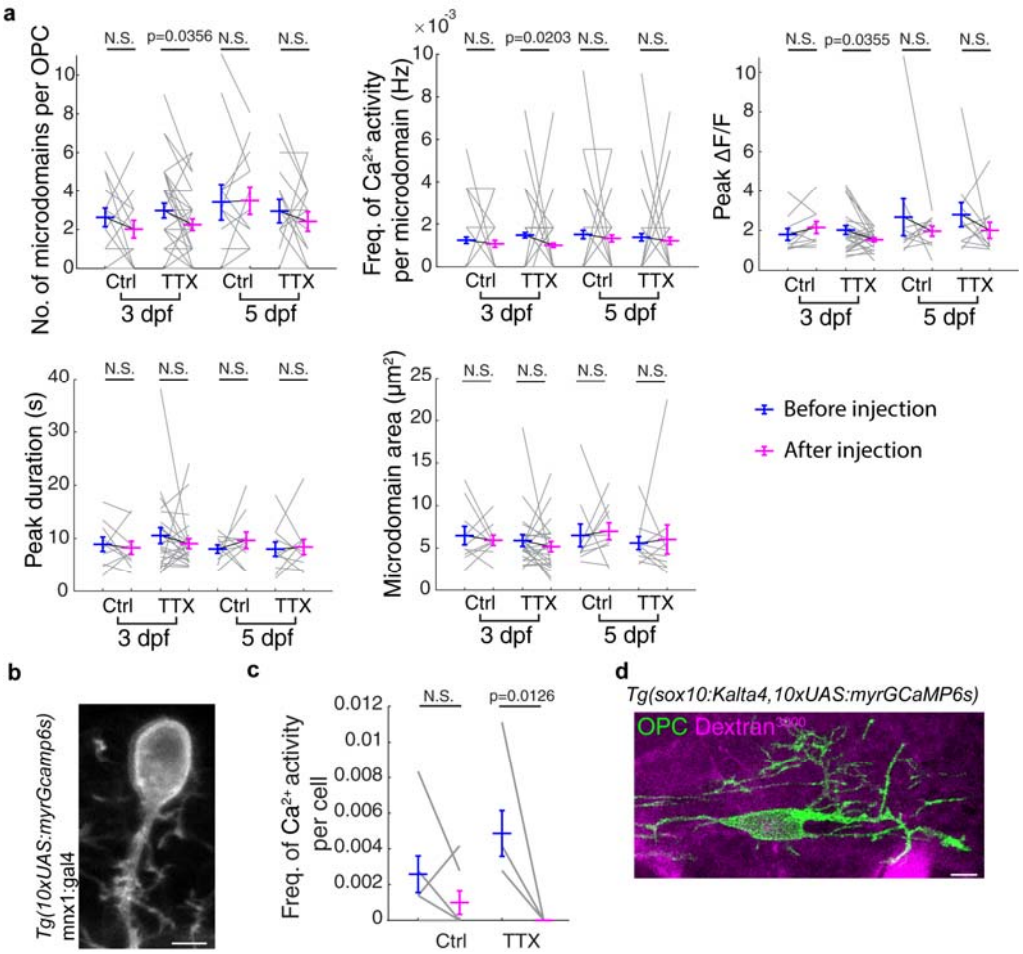

726

727 ***Extended Data Figure 7. TTX has limited effects on intrinsic OPC Ca^{2+} activity at 3 dpf but not 5 dpf.***
728 **a**, Quantification of Ca^{2+} microdomain number per OPC, frequency of Ca^{2+} activity per microdomains,
729 peak amplitude, peak duration, and area of Ca^{2+} microdomain in OPCs before (blue) and after (magenta)
730 injection of 1 nL of control or TTX (0.5 mM) solution. Paired data indicated with grey line.
731 *Tg(sox10:Kalta4,10xUAS:myrGCaMP6s)* larvae at 3- and 5 dpf were analyzed. From left, n = 15 ,31, 13
732 and 17 cells from 7, 13, 6 and 9 fish. **b**, Representative images of primary motoneurons visualized by
733 injecting *mnx1:gal4* into *Tg(10xUAS:myrGCaMP6s).* **c**, Quantification of frequency of Ca^{2+} activity per cell
734 before (blue) and after (magenta) TTX injection in motoneurons at 5 dpf. n = 7 and 6 cells from 5 and 5
735 fish. **d**, Representative image of an OPC surrounded by dextran MW3000 by the time of imaging after
736 TTX injection. All data are represented as mean ± SEM; N.S., not significant; paired *t*-test; Scale bar 5 µm.
737

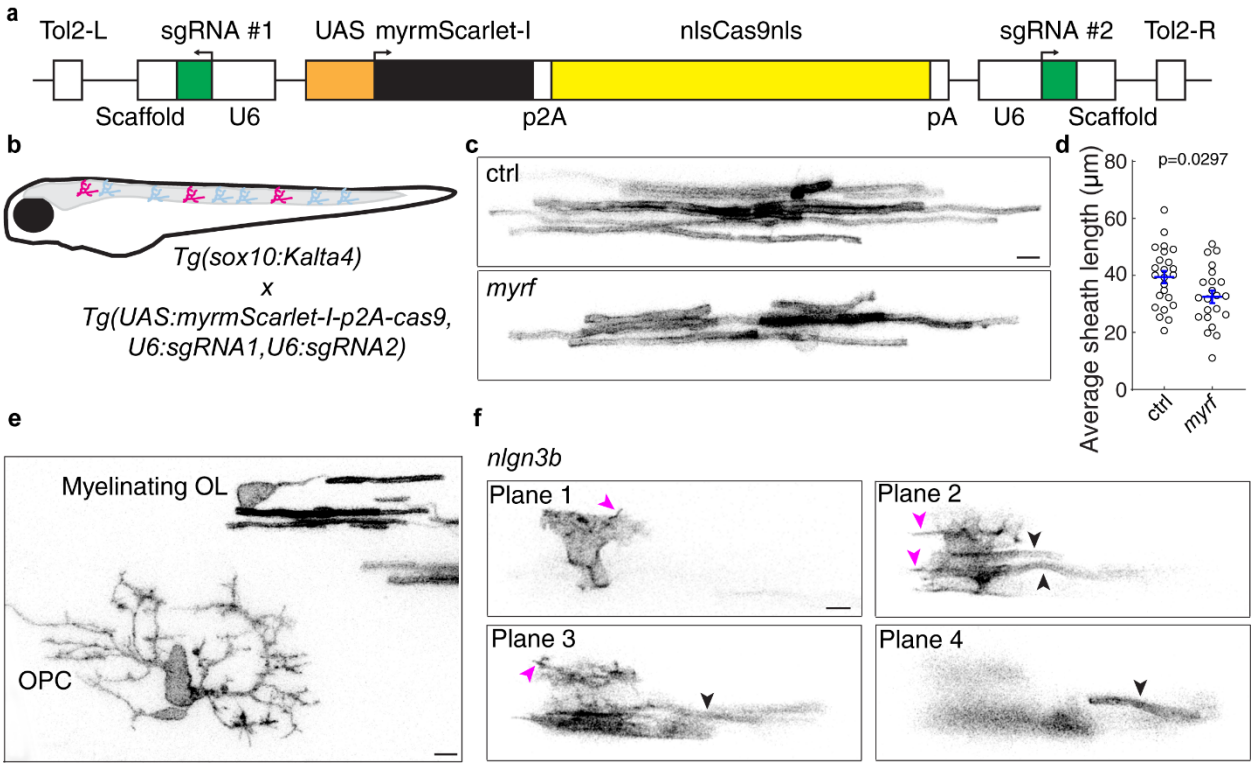

Extended Data Figure 8. A cell-specific knockdown approach effectively disrupts oligodendrocyte development. **a**, Schematic of Tol2 plasmid (10xUAS:myrmScarletI-p2A-Cas9, U6:sgRNA1;U6:sgRNA2) constructed and used to induce cell-specific Cas9 expression with membrane labeling and 2 separate U6-driven sgRNAs. **b**, Schematic of larva with sparsely labeled oligodendrocytes resulting from *Tg(sox10:Kalta4)* crossed with transgenic fish carrying the plasmid from (**a**). **c**, Representative images of single myelinating oligodendrocyte in the spinal cord of *Tg(10xUAS:myrmScarletI-p2A-Cas9, U6:ctrl-sgRNA1;U6:ctrl-sgRNA2)* and *Tg(10xUAS:myrmScarletI-p2A-Cas9, U6:myrf*^{ex3}*-sgRNA;U6:myrf*^{ex4}*-sgRNA)* at 6 dpf. **d**, Quantification of myelin sheath length from (**c**). n = 24 and 22 cells from 15 fish. **e**, Representative image of an OPC and a myelinating oligodendrocyte (OL). **f**, 4 single planes of a trapezoid-shaped process in an otherwise myelinating OL in *nlgn3b*-targeted larvae at 5 dpf. Myelin sheaths indicated by black arrowheads and processes by magenta arrowheads. All data are represented as mean ± SEM; N.S., not significant; unpaired *t*-test; scale bar 5 µm.

Supplementary information

Supplementary video 1. Time-lapse images of PSD-95-GFP in an OPC.
Representative video of sox10:myrTagRFP-T-P2A-PSD95-GFP in an OPC from the spinal cord of a 3 dpf larva. GFP-Gephyrin (magenta) puncta are dynamic in location and size, while the OPC processes are relatively stable (cyan).

Supplementary video 2. Time-lapse images of PSD-95-GFP in a neuron.
Representative video of 10xUAS:PSD95-GFP in a neuron in the spinal cord of a *Tg(sox10:Kalta4)* larva at 3 dpf.

Supplementary video 3. Time-lapse images of GFP-Gephyrin in an OPC.
Representative video of sox10:myrTagRFP-T-P2A-GFP-Gephyrin in an OPC from the spinal cord of a 3 dpf larva. GFP-Gephyrin (magenta) puncta are dynamic in location and size, while the OPC migrates and remodels its processes (cyan).

Supplementary video 4. Time-lapse images of GFP-Gephyrin in a neuron.
Representative video of 10xUAS:GFP-Gephyrin in a neuron in the spinal cord of a *Tg(sox10:Kalta4)* larva at 3 dpf.

Supplementary video 5. Time-lapse images of myrGCaMP6s in an OPC.
Representative video of Ca^{2+} activity in an OPC in a *Tg(olig1:Kalta4,10xUAS:myrGCaMP6s)* larva at 5 dpf.

Supplementary video 6. Time-lapse images of myrGCaMP6s in an OPC reveal somal Ca^{2+} activity.
Video of Ca^{2+} activity in an OPC with multiple events including a single somal event in a *Tg(olig1:Kalta4,10xUAS:myrGCaMP6s)* larva at 5 dpf.

Supplementary video 7. Time-lapse images of myrGCaMP6s in an OPC before and after injection of control solution.
Representative 20 min-video of Ca^{2+} activity in an OPC before and after injection of control solution in a *Tg(olig1:Kalta4,10xUAS:myrGCaMP6s)* larva at 5 dpf. Yellow arrows indicate the Ca^{2+} events.

Supplementary video 8. Time-lapse images of myrGCaMP6s in an OPC before and after injection of cadmium.
Representative 20 min-video of Ca^{2+} activity in an OPC before and after injection of cadmium in a *Tg(olig1:Kalta4,10xUAS:myrGCaMP6s)* larva at 5 dpf. Yellow arrows indicate the Ca^{2+} events.

Supplementary video 9. Time-lapse images of myrGCaMP6s in an OPC before and after injection of TTX at 3 dpf.
Representative 20-minute video of Ca^{2+} activity in an OPC before and after injection of TTX in a *Tg(sox10:Kalta4,10xUAS:myrGCaMP6s)* larva at 3 dpf. Yellow arrows indicate the Ca^{2+} events.

Supplementary Table 1. A list of primers used in this study.
Supplementary Table 2. Statistical information.
Supplementary Table 3. Fish used for experiments.

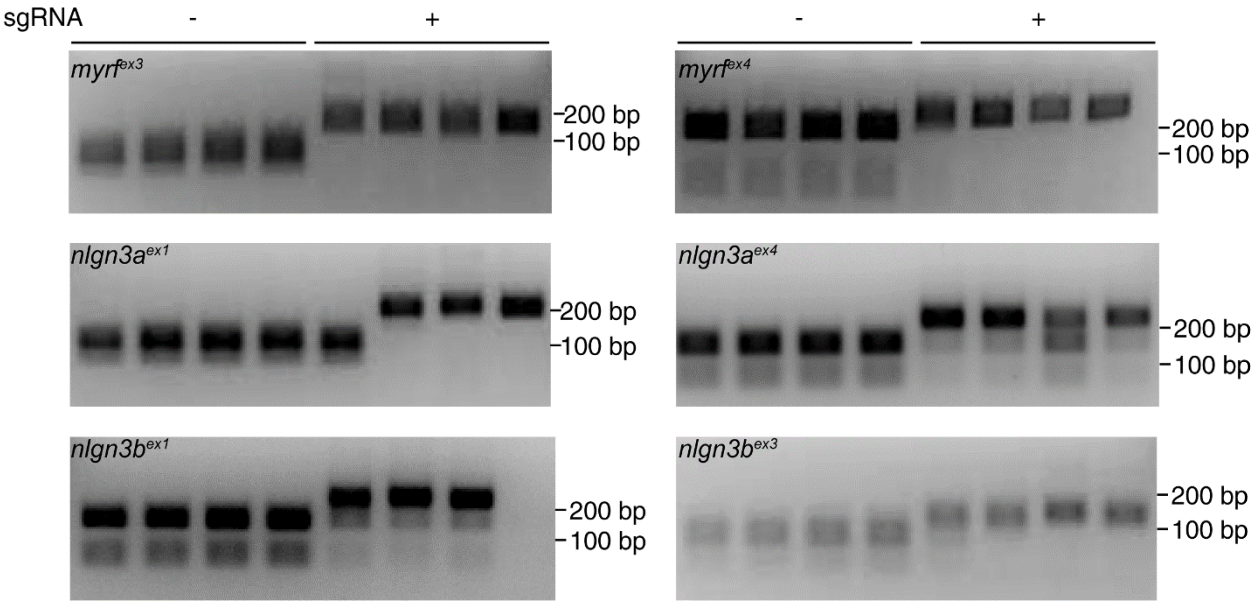

802

803 ***Supplementary Figure 1. Selected sgRNAs are efficient cutting targeted genomic regions.***
804 Representative gel images of digested PCR product of genomic regions targeted by the sgRNAs. Each
805 lane represents a single embryo at 1 dpf. The left 4 lanes are uninjected (-) and the right 4 lanes are
806 injected (+) with sgRNAs and Cas9 protein.
807
808